The Relative Distance between the Clusters of Galaxies A2634 and Coma [1]

Marco Scodeggio, Riccardo Giovanelli and Martha P. Haynes
Center for Radiophysics and Space Research and National Astronomy and Ionosphere Center,
Cornell University, Ithaca, NY 14853
scodeggi, riccardo, haynes@astrosun.tn.cornell.edu

ABSTRACT

The Tully-Fisher (TF) and Fundamental Plane (FP) relations are used to obtain two independent estimates of the relative distance between the clusters A2634 and Coma. Previously published studies of A2634 showed a large discrepancy between the distance estimates obtained with the TF and the $D_n - \sigma$ relations, questioning the reliability of redshift-independent distances obtained using these relations. Because of the importance of this issue, we have obtained new distance estimates for A2634, based on much larger samples than previously used, and selected according to rigorous membership criteria. New I band CCD photometry for 175 galaxies, new 21 cm observations of 11 galaxies, and new velocity dispersion measurements for 62 galaxies are used together with previously published data in building these samples.

As part of a larger project to compare the TF and FP distance-scales, we have obtained a new FP template using for the first time I band photometry. The template is derived using a sample of 109 E and S0 galaxies that are members of the Coma cluster. Its parameters are in very good agreement with recent determinations of the FP obtained at shorter wavelengths. The uncertainty with which the FP can provide peculiar velocity estimates for single galaxies is $\simeq$0.43 mag in the distance modulus, or 20% of the distance. This uncertainty is slightly larger than the typical uncertainty that characterizes TF estimates. However this disadvantage is partly compensated by the fact that the sample incompleteness bias has a less severe effect on FP cluster distance estimates than it has on the corresponding TF distance estimates. Also, cluster membership is more readily established for early–type objects than for spirals.

After the appropriate corrections for sample incompleteness have been taken into account, we find the TF and FP distance estimates to be in good agreement, both indicating that A2634 has a negligibly small peculiar velocity with respect to

[1] Work based in part on observations obtained at the Arecibo (AO), Kitt Peak (KPNO) and Palomar (PO) Observatories. Observations at the PO were made as part of a continuing collaborative agreement between the California Institute of Technology and Cornell University. The AO is part of the National Astronomy and Ionosphere Center, which is operated by Cornell University under a cooperative agreement with the National Science Foundation. The KPNO is part of the National Optical Astronomical Observatories, which are operated by Associated Universities, Inc. under a cooperative agreement with the National Science Foundation.

the Cosmic Microwave Background reference frame. Because of the high accuracy with which the two distance estimates have been obtained, their agreement strongly supports the universality of the TF and FP relations, and therefore their reliability for the estimate of redshift-independent distances.

1. Introduction

The measurement of redshift-independent distances, together with that of redshift measurements, constitutes one of the basic tools of observational cosmology. While redshift surveys alone can be used to obtain maps of the distribution of luminous matter in the local Universe (see Giovanelli & Haynes 1991 for a recent review), only redshift-independent distances can dynamically constrain the total matter content (i.e. dark plus luminous) of the Universe. In the absence of perfect "standard candles", i.e. objects of well determined and invariant intrinsic properties, many different methods have been developed to climb the "distance scale ladder" out to cosmologically significant distances (see for example Rowan-Robinson 1985). The ideal method would provide high accuracy, i.e. it would exhibit small dispersion in the predicted distance, it would be applicable over a large range of distances and for a well distributed set of targets, and it would have a well understood physical base. So far no technique has been developed that satisfies all of the above requirements. Among the available methods (see Jacoby *et al.* 1992 for a review), those most extensively utilized are the Tully-Fisher (TF) relation (Tully & Fisher 1977), which is applied to spiral galaxies, and the $D_n - \sigma$ or Fundamental Plane (FP) relation (Dressler *et al.* 1987; Djorgovski & Davis 1987), which is applied to elliptical and lenticular galaxies.

TF, FP and $D_n - \sigma$ are very similar methods, all based on the correlation between a photometric distance-dependent parameter and a spectroscopic, distance-independent quantity. The three relations have fair accuracy (the uncertainty in the distance prediction of a single galaxy is 12 – 25%), and they can be applied over a large distance interval (from the Local Group out to galaxies with redshift greater than 0.1; see for example Franx 1993; Vogt *et al.* 1993, Vogt *et al.* 1996, van Dokkum & Franx 1996). Although they can be generically understood in terms of virial equilibrium, the astrophysical details of these relations are obfuscated by the variance in the formation and evolution histories of galaxies. The calibration of the relations is thus a purely empirical exercise. Also, because of the uncertainty on the value of the Hubble constant, and because the number of nearby galaxies that could be used for an absolute calibration of the template relations is very small, these relations are most commonly used to derive only relative distances. In the following, the term distance is therefore used as an abbreviation for the more appropriate "recession velocity corrected for peculiar motions".

It is well known that in the absence of a perfect standard candle, distance measurements are subject to bias, arising from a variety of sources (see Teerikorpi 1984,1990,1993; Sandage 1994a,b; Willick 1994; Giovanelli *et al.* 1996b; and references therein). Bias corrections thus play an important role in the measurement of peculiar velocities. It is also possible that the environment

might have an effect. For example, the template TF, $D_n - \sigma$, or FP relation might depend on the local density of galaxies, and thus differ among rich and poor clusters, and between clusters and the field. Yet again, the intrinsic scatter about the mean relation might be coupled with the space distribution of galaxies, complicating the bias correction procedures.

It is then legitimate to ask whether the TF, $D_n - \sigma$ and FP are universal relations. Some attempts have been made toward quantifying this issue (Aaronson *et al.* 1986; Djorgovski, De Carvalho & Han 1988; Guzmán *et al.* 1992; Jørgensen, Franx & Kjærgaard 1996), producing however conclusions of marginal clarity.

An invalid or biased template relation will yield spurious peculiar velocities. It has even been argued, for example, that the very evidence suggesting the existence of a Great Attractor (Dressler *et al.* 1987, Lynden-Bell *et al.* 1988) might result from bias (Silk 1989). A comparison by Mould *et al.* (1990) between cluster peculiar velocities obtained by respectively using the TF and $D_n - \sigma$ techniques shows disagreement which exceeds that expected from the reported uncertainties associated with the two methods. The case of A2634, pointed out by Lucey *et al.* (1991a; hereafter L91a), is even more notorious: Aaronson *et al.* (1986, hereafter A86) applied the TF relation to find the cluster roughly at rest in the Cosmic Microwave Background (CMB) reference frame, while L91a used the $D_n - \sigma$ relation to obtain a cluster peculiar velocity of –3400 $\mathrm{km\,s^{-1}}$. The difference between the two estimates is significantly larger than the combined uncertainty of the two separate results (approximately a 5σ discrepancy), leading L91a to conclude that environmental effects in this cD–dominated cluster might be responsible for systematic bias in the properties of the early-type galaxy population. In such case, *$D_n - \sigma$ and FP would not be universal relations, and they could not be used to reliably map the peculiar velocity field.*

Other possible explanations for the discrepancy in A2634 should be considered. The A86 and L91a samples have very different spatial distributions, prompting the doubt that early- and late-type galaxies may not sample the same dynamical unit. The L91a sample is composed of 18 E and S0 galaxies in the core of A2634 (all galaxies are at a radial distance of ≤ 0.2 deg from the cluster center), while the A86 sample is composed of 11 spiral galaxies scattered over a large area, several degrees to the side, that includes not only A2634 but also the cluster A2666. Scodeggio *et al.* (1995, hereafter S95) have shown that only 7 galaxies in the A86 sample are proper members of A2634, while the remaining 4 are foreground objects. In addition, both the A86 and L91a studies failed to apply bias corrections.

Because of the important concerns raised by the previously mentioned results, it appeared desirable to carry out a new detailed and multi–pronged study of A2634, which would satisfactorily answer the issues of sample adequacy and template relation universality. In a previous paper (S95) we presented the results of the first part of our study of A2634, which aimed at easing sample selection concerns. There, an extensive redshift survey provided a detailed kinematical and dynamical analysis of the A2634 region. The ensuing ability to characterize cluster membership accurately (a) suggested that the loose sample selection criteria of A86 did not seriously affect

their inferred peculiar velocity, and (b) was used to select two samples, one of E + S0 and one of spiral galaxies, that are used here to derive new peculiar velocity estimates of A2634. For the spiral sample, the motion of A2634 is referred to the template relation recently obtained by Giovanelli *et al.* (1996b; hereafter G96b), based on 24 clusters. Since such a template is not yet available for early-type galaxies, we refer the motion of A2634 inferred from the FP relation to a template obtained using the Coma cluster. For that purpose, in both A2634 and Coma we have obtained new photometric observations, and new velocity dispersions to supplement the data already available in the literature. In a forthcoming work (Scodeggio, Giovanelli & Haynes 1996) we will present a more accurate derivation of the FP template, based on a multi-cluster sample, and extend the comparison of the TF and FP distance-scales to a larger sample of nearby clusters.

The remainder of this paper is organized as follows. In § 2 we discuss cluster membership. In § 3 we present our new spectroscopic and photometric observations. In § 4 we briefly discuss the incompleteness bias correction. In § 5 we present the new TF and FP distance estimates and in § 6 we summarize the main results of this work.

Throughout the paper we parameterize distance–dependent quantities via $H_\circ = 100h$ km s^{-1} Mpc^{-1}.

2. Cluster membership

Reliable assignment of cluster membership is an important criterion in the definition of a TF or FP sample for a cluster of galaxies. Because of the sparse character of the spiral population in clusters, TF samples often fail strict membership criteria. Poor knowledge of the cluster structure or the need to restrict to the brightest objects, has led observers to draw targets from wide regions around cluster centers in order to maximize target counts. In this study we aim to overcome such limitations.

The properties of Coma and A2634 are well known and we summarize them in Table 1. Thanks to the availability of a large body of galaxy redshifts, detailed kinematical and dynamical studies of both clusters are available. The Coma cluster was first studied in detail by Kent & Gunn (1982), and redshift space caustic curves that mark the separation between the gravitationally bound cluster members and the unbound "field" have been published, most recently by Regös & Geller (1989) and Gavazzi, Randone & Branchini (1995). The cluster is well separated in redshift space from both the foreground and the background field, and membership can be reliably assigned to objects to an angular separation of approximately 5 degrees from the cluster center. Following the criterion used by Giovanelli *et al.* (1996a; hereafter G96a), we define as cluster members all galaxies within 4 degrees from the cluster center that fall within the radial velocity limits defined by the Regös & Geller (1989) caustic curves estimated for $\Omega_\circ = 0.3$. The substructure within the Coma cluster recently discussed by Colless & Dunn (1996) appears to be insignificant for our discussion. The difference in distance between the merging units, as inferred by these authors, is a

negligible fraction of the distance to the Coma cluster, and would produce, at most, only a small increase in the scatter of of the TF and FP diagrams for this cluster.

The first in–depth redshift survey of A2634 was carried out by Pinkney *et al.* (1993). A more detailed study of the cluster structure was carried out by S95, which also estimated redshift space caustic lines. A2634 is located in a region of higher complexity than that containing Coma. The cluster A2666 (cz_{hel} = 8,134 $km\,s^{-1}$) lies 3° to the East of A2634 (cz_{hel} = 9,240 $km\,s^{-1}$); two more groups, one in the foreground (cz_{hel} = 7,546 $km\,s^{-1}$) and one in the background (cz_{hel} = 11,619 $km\,s^{-1}$), were identified by S95, projected respectively 1.1 and 0.6 degrees to the NE and to the SE of A2634. In addition, two background clusters, A2622 at cz_{hel} = 18,345 $km\,s^{-1}$, and an anonymous cluster at cz_{hel} = 37,093 $km\,s^{-1}$, are projected to within less than 1 degree from the center of A2634. We define as A2634 members all galaxies within 2.5 degrees from the cluster center that fall within the radial velocity limits defined by the S95 caustic curves corresponding to $\Omega_\circ = 0.3$.

In addition to the strict cluster members, we include in our samples also a number of galaxies that we classify as "peripheral members". These are galaxies with radial velocity very close to the cluster systemic velocity, but sufficiently removed from the cluster center that they do not satisfy a strict membership criterion. In the following paragraph, the term cluster members will be used to indicate both the strict cluster members and the peripheral ones.

3. Observations and Data Sets

The selection of the Coma TF sample is described in G96a. The sample includes 41 galaxies, of morphological type between Sb and Sd, and with inclination greater than 45°, that satisfy the membership criteria discussed in the previous paragraph. The A2634 TF and FP samples are based on the catalog of the redshift survey by S95. The TF sample was selected following the same criteria as in the Coma case, except that it includes two galaxies with inclination lower than 45°, and one Sa galaxy. Two very late spiral or irregular galaxies with serendipitously measured widths are also included in this sample, for a total of 27 galaxies. Both the Coma and the A2634 FP samples were selected to satisfy membership criteria. The Coma sample is composed of 109 galaxies, 71 ellipticals and 38 lenticulars, while the A2634 one is composed of 55 galaxies, 22 ellipticals and 33 lenticulars. Three galaxies were found to show some indication of spiral structure, and have been tentatively classified as Sa in Tables 3 and 4.

3.1. Arecibo Observations

In addition to the data presented in G96a, measurements for 11 spiral galaxies in the A2634 TF sample are included here. Velocity widths were obtained from 21 cm observations carried out between 1990 and 1994 with the Arecibo 305m radio telescope. The observational setup was as

described in Giovanelli & Haynes (1989). Since this sample includes galaxies significantly fainter than those customarily observed in 21 cm emission, integration times averaged 0.7 hours per object on source. The typical rms noise per channel ranged from 0.3 to 0.9 mJy. All observations were taken with a spectral resolution of approximately 8 $\mathrm{km\,s^{-1}}$, later reduced by smoothing by an amount dependent on the signal-to-noise ratio. The velocity width was measured using an algorithm that fits the rising sides of the galaxian profile with low order polynomials, and obtains the width at a 50% level of each of the profile horn peaks or single peak, depending on the line shape. We refer the reader to the discussion in G96a for further details.

3.2. Kitt Peak observations

Photometric parameters for 175 galaxies were derived from I band CCD images obtained with the 0.9m telescope of the Kitt Peak National Observatory (KPNO), during 3 observing runs between April 1994 and September 1995, plus some service observing by KPNO personnel in August 1993 (A2634 only). The telescope was used with the f/7.5 secondary, field corrector and T2KA CCD chip (2048 x 2048 pixels), to obtain a field of view of $23'$ x $23'$, with a spatial scale of $0.68''$ per pixel. All frames were obtained with 600 seconds integration time. The median seeing (measured as the FWHM of the stellar light profile) for the observations presented here was $1.5''$. The cores of the clusters were mapped with a mosaic of frames in a regularly spaced grid, while specific pointings were used for target galaxies at the clusters periphery. Observations of Landolt fields (Landolt 1992), both at I and at R band, were repeated many times during each night, at airmasses between 1.2 and 2.5, to provide the photometric calibration. The mean uncertainty in the zero point calibration at I band was 0.021 magnitudes. The 1993 service observing frames were obtained in non-photometric conditions, and have been calibrated "a posteriori", using overlapping sky regions between those frames and frames obtained in photometric conditions during the Sept. 1994 and Sept. 1995 runs. An average of 15 stars was used to calibrate each frame, with mean uncertainty of 0.028 magnitudes.

The data reduction process was performed using standard IRAF[2] procedures, and the GALPHOT surface photometry package written for IRAF/STSDAS[3] by W. Freudling, J. Salzer, and M.P. Haynes. All frames have been bias-subtracted and flat-fielded using a "superflat" obtained combining, with a median filter, a large number (≥ 50) of frames. For each galaxy, a local sky background was determined as the mean number of counts measured in 10-12 regions of "empty" sky, and subtracted from the frame. The typical uncertainty in this mean background,

[2]IRAF (Image Reduction and Analysis Facility) is distributed by NOAO, which is operated by the Association of Universities for Research in Astronomy, Inc. (AURA), under cooperative agreement with the National Science Foundation.

[3]STSDAS (Space Telescope Science Data Analysis System) is distributed by STScI, which is operated by AURA, under contract to the National Aeronautics and Space Administration.

determined from the differences in the sky value obtained for galaxies in the same frame, is approximately 0.2%. All pixels contaminated by the light of foreground stars or nearby galaxies, or by cosmic rays hits, were blanked, and excluded from the final steps of surface photometry. A galaxy's light distribution was fitted with elliptical isophotes using a modified version of the STSDAS *isophote* package, maintaining as free parameters the ellipse center, ellipticity and position angle, and incrementing the ellipse semi-major axis by a fixed fraction of its value at each step of the fitting procedure. The fitted parameters yield a model of the galaxy, which in turn is used to compute integrated magnitudes as a function of semi-major axis.

The outer part of the surface brightness profiles of spiral galaxies were fitted with an exponential disk. This fit was used to extrapolate the disk profile to infinity, and to define the interval of radii where the mean disk ellipticity is to be computed. The latter was then used to derive the galaxy inclination. Total magnitudes were obtained adding the flux corresponding to the extrapolated part of the disk profile to the flux measured within the outermost fitted elliptical isophote, and have a median uncertainty of 0.04 magnitudes. The uncertainty on the ellipticity is a function of inclination itself, and can vary from 1 to 20%, as shown in G96a. The surface brightness profile of each early-type galaxy was fitted with a de Vaucouleurs $r^{1/4}$ profile, yielding an effective radius r_e and effective surface brightness μ_e (the mean surface brightness within r_e). The fit was performed from a radius equal to twice the seeing radius, out to the outermost isophotes for E galaxies; for S0 and S0a galaxies only the central core was fitted . Total magnitudes were obtained by extrapolating the $r^{1/4}$ fit to infinity (E galaxies), or by extrapolating to infinity the exponential profile that fitted the outer parts of the galaxy light profile (S0 and S0a galaxies), and adding the flux corresponding to the extrapolated part of the profile to the one measured within the outermost fitted galaxy isophote. The median uncertainty on the determination of r_e is 5%, and 0.06 mag on that of μ_e.

For galaxies in close galaxy pairs, and for brightest cluster members and the smaller companions embedded in their halos, an iterative subtraction procedure was used to obtain the individual galaxy light profiles. First, the brighter object was fitted, after the fainter one(s) was blanked. The fit was then used to build a model of the brighter galaxy, which was subtracted from the original image. The subtracted image was used to fit the fainter object, and then to build a model for it; the latter was then subtracted from the original image and the bright object fitted again. The procedure converged usually at the second iteration, producing companion-subtracted light profiles, though the uncertainty on μ_e was higher than in other cases.

3.3. Palomar Observations

Stellar velocity dispersion measurements for 62 early-type galaxies in our FP samples were obtained from moderate dispersion optical spectra. All spectroscopic observations were obtained with the Hale 5m telescope of the Palomar Observatory, during 4 observing runs between September 1992 and September 1994. The red camera of the Double Spectrograph (Oke & Gunn

1982) was used with a 1200 lines mm^{-1} grating and a $2''$ x $128''$ slit to obtain spectra with a dispersion of 0.86 Å per pixel, and a resolution of 2.2 Å (corresponding to a velocity resolution of 129 $km\,s^{-1}$ at 5300 Å). The spectral coverage was approximately from 5000 to 5600 Å, centered on the Mg Ib lines at ∼5175 Å. Exposure times ranged from 15 to 90 minutes, depending on the brightness of the target galaxy, with a median value of 30 minutes. The slit was kept to an East-West orientation, unless a close galaxy pair was being observed, and both spectra were recorded simultaneously. HeNeAr lamp spectra were obtained before and after each galaxy observation, to provide wavelength calibration. Late G and early K type giant stars were used as velocity standards and as templates for the velocity dispersion measurements.

All spectroscopic data were reduced using standard IRAF procedures. All frames were bias-subtracted and flat-fielded using normalized dome flat-fields. No correction for the slit profile was necessary. Cosmic ray hits were removed interactively from all frames. Because approximately half of the observations were performed in non-photometric conditions, the spectra were not flux-calibrated. The wavelength calibration was obtained in two steps. First, the HeNeAr lamp spectra frames were used to obtain a two-dimensional dispersion solution. Typically 12-14 spectral lines, spread uniformly over the entire spectral range, were used in the fit. The r.m.s. deviations between true and fitted wavelength were between 0.06 and 0.1 Å. The galaxy spectra were then transformed to linear dispersion using the lamp dispersion solution. Next, the two strong night-sky lines at 5460.7 and 5577.4 Å were used to check the absolute wavelength calibration. In a small number of cases where the original calibration was not satisfactory, the wavelength solution was rigidly shifted to bring the two sky lines in agreement with their expected wavelength. Finally the global consistency of the wavelength calibration procedure was verified using the velocity standard stars. Radial velocities were measured repeatedly for all stars, using in turn one star as template and all others as unknown. The r.m.s. dispersion in the differences between true and measured velocities, considering spectra obtained in all 4 observing runs, is approximately 9 $km\,s^{-1}$, in good agreement with the measured uncertainty in the wavelength of the two sky lines.

One-dimensional galaxy spectra, to be used for the velocity dispersion determinations, were extracted using a $6''$ wide window (in the cross-dispersion dimension), centered on the peak of the galaxy continuum. All measurements of velocity and velocity dispersion were obtained using the cross-correlation technique of Tonry & Davis (1979), implemented in the IRAF task *fxcor*. The basic assumption of this and other similar methods (Sargent *et al.* 1977, Franx Illingworth & Heckman 1989, Bender 1990) is that the spectrum of an early-type galaxy is well approximated by the spectrum of its most luminous stars (K0 – K1 giants), modified only by the effects of the stellar motions inside the galaxy. Since these motions introduce only a Doppler shift in the stellar spectra, the galaxy spectrum is given by the convolution of the spectrum of a K giant star with the line of sight stellar velocity distribution (LOSVD). Therefore the LOSVD can be obtained by deconvolving the galaxy spectrum. This task was done in the Fourier transform domain, where convolution and cross-correlation reduce to a product. Before the Fourier transform was computed, all spectra and templates were continuum-subtracted, normalized, end-masked with a

cosine bell function, and logarithmically re-binned.

Because of the limited signal-to-noise ratio of the spectra, and in order to facilitate comparisons with other studies, we constrained the deconvolution procedure by assuming that the LOSVD is Gaussian, and therefore characterized by two parameters only: a mean velocity and a velocity dispersion σ. The accuracy of the procedure was determined using simulated galaxy spectra. We broadened stellar template spectra with Gaussian profiles that simulate a large range of velocity dispersions, added Poissonian noise to the broadened spectra, and then measured the velocity dispersion using the original spectrum as the template. These tests showed that *fxcor* produces an overestimate of the velocity dispersion at the 4–5% level, and therefore we have corrected the raw measurements to remove this effect. The final velocity dispersion values were obtained by averaging the determinations obtained with five different stellar templates, of spectral types between G9 and K2.

Given the relatively large size of the extraction window, it is possible that galaxy rotation, if present, might contribute some significant broadening of the spectral lines, and bias the velocity dispersion measurements. We have obtained rough estimates of the galaxy rotation velocity, and of its contribution to the line broadening, using the original two-dimensional spectra. A five points rotation curve within the $6''$ extraction aperture was obtained for each galaxy, based on 1-dimensional spectra extracted using 2-pixel wide apertures positioned side by side. The differences in the radial velocity measured in each one of the four lateral spectra, and the one measured in the central one, define the projection of the rotation curve along the slit, which was arbitrarily oriented in the E–W direction. The contribution from rotation to the line broadening was estimated using a very simple model. A galaxy spectrum was simulated combining 5 copies of a stellar template spectra, broadened with a Gaussian of fixed width, and shifted to reproduce the 5 velocities in the rotation curve. The weights used in the combination were derived from the relative intensities in the continuum of the 5 spectra used to determine the rotation curve. The comparison of the velocity dispersion measured in the simulated spectrum with the one used to broaden the stellar templates provides an estimate of the amount of broadening due to rotation.

Given the accuracy with which we can measure radial velocities in our spectra, and the small number of points used to derive the rotation curve, we cannot reliably measure rotation velocities smaller than $\simeq$25 $\mathrm{km\,s^{-1}}$. Within the A2634 and Coma samples presented here (62 galaxies), 21 galaxies do not show detectable rotation, while the remaining 41 have a median rotation velocity of 49 $\mathrm{km\,s^{-1}}$, with the largest measured rotation velocity being 132 $\mathrm{km\,s^{-1}}$. This rotation is responsible for an average broadening of the LOSVD of $\simeq$2%, with a maximum of $\simeq$7% for the largest rotation velocity. The velocity dispersions listed in Table 3 and 4 are corrected for this effect.

Our spectroscopic sample partly overlaps those presented by L91a for A2634, and by Lucey *et al.* (1991b, hereafter L91b), Davies *et al.* (1987), and Faber *et al.* (1987) for Coma. We can therefore compare the different velocity dispersion scales, and eventually merge all spectroscopic

observations in a single database. For Coma, we have 6 velocity dispersion measurements in common with Davies *et al.* (1987) and Faber *et al.* (1987), and 6 measurements in common with L91b. In both cases the mean difference between measurements is $\simeq$1%, with a dispersion of $\simeq$10%, which is close to the expected value obtained combining the quoted uncertainties of the single measurements. For A2634 we have 7 velocity dispersion measurements in common with L91a. Our measurements are systematically smaller, by 14% on average, although much of this discrepancy is due to just two galaxies (330649 and 330678, L91a objects 1482 and 134). For these two objects our velocity dispersions are 24% smaller than those published by L91a. Figure 1 shows the comparison between our measurements and those found in the literature. Filled symbols identify galaxies in the Coma cluster, while empty symbols identify the galaxies in A2634 that we have in common with L91a. Given the good agreement between the different measurements, and because the small number of objects in common with the L91a sample prevents an accurate determination of any possible offset in the L91a velocity dispersion scale, in the following we use the L91a, L91b, Davies *et al.* (1987), and Faber *et al.* (1987) velocity dispersion measurements as reported in the literature, and combine them with the new measurements presented here.

3.4. TF and FP samples

Both A2634 and Coma are included in the cluster sample of G96a and G96b. Because no new TF observations are presented here for the Coma cluster, we do not discuss that sample again (all the data can be found in Table 2 in G96a). New TF observations have been obtained for 11 galaxies in A2634, and we present them in Table 2, together with the sample of G96a, giving a complete list of the TF sample for that cluster. Table 2 is organized as follows:
Col. 1: Galaxy name, using one or two galaxy identifiers. If the galaxy is listed in the UGC catalog, the UGC number is listed first; if not, our internal coding number is given. The second identifier is the NGC or IC number, if the galaxy is listed in those catalogs, or the CGCG field and ordinal number within that field, if the galaxy is listed in the CGCG. If the galaxy is neither an NGC/IC nor a CGCG object, no second name is entered.
Cols. 2 and 3: Right Ascension and Declination, in 1950.0 epoch.
Col. 4: morphological type code, in the RC3 scheme (1 for Sa, 3 for Sb, 5 for Sc, 10 for Irr). Morphological types were derived from visual inspection of the blue plates of the Palomar Observatory Sky Survey (POSS).
Col. 5: Radial velocity, in $\mathrm{km\,s^{-1}}$, measured in the CMB reference frame as defined by Kogut *et al.* (1993).
Col. 6: Angular distance from the cluster center, in degrees.
Col. 7: Membership code: A2634 members according to S95 are identified by a "c"; peripheral objects are identified by a "g"; members of S95 foreground group at cz = 7500 $\mathrm{km\,s^{-1}}$ are identified by a "7".
Col. 8: Observed velocity width, in $\mathrm{km\,s^{-1}}$. Velocity widths are derived either from either 21 cm observations or from optical rotation curves, as described in G96a. To that source we address

the reader for details on the corrections applied for instrumental, reduction, and relativistic broadening, turbulent motion, and inclination.
Col. 9: Velocity width, in $\mathrm{km\,s^{-1}}$, corrected for turbulent broadening, instrumental and data taking effects, cosmological stretch, and shape of the optical rotation curve, but not for inclination.
Col. 10: Velocity width, in $\mathrm{km\,s^{-1}}$, corrected for inclination.
Col. 11: Inclination, in degrees. A galaxy inclination is given by $\cos^2 i = \frac{(1-e_{corr})^2-q^2}{1-q^2}$ where e_{corr} is the mean ellipticity of the disk, corrected for the smearing effects of seeing (see Giovanelli *et al.* 1995), and q is the intrinsic axial ratio of spiral disks (we assume $q = 0.13$ for Sbc and Sc galaxies, and $q = 0.2$ for all other types).
Col. 12: Logarithm (base 10) of the corrected velocity width, and its associated uncertainty. The format 2.377(13) should be read as 2.377±0.013.
Col. 13: Measured apparent I band total magnitude.
Col. 14: Corrected I band magnitude. Total magnitudes are corrected for extinction within our Galaxy (adopting Burstein & Heiles 1978 prescriptions, and $A_I = 0.45A_B$), for the cosmological k-correction term (adopting Han 1992 $k_I = 0.16z$) and for internal extinction. This is done following the prescriptions of G96A, with the correction to face-on value that depends on the galaxy inclination, and also on its luminosity.
Col. 15: Absolute magnitude. This is obtained assuming that the galaxy is at the distance indicated by the cluster redshift, in the CMB reference frame, for the objects labeled "c" in col. 7, and at a distance indicated by the galaxy redshift, for the other objects, for $\mathrm{H_\circ}$=100 km $\mathrm{s^{-1}}$ $\mathrm{Mpc^{-1}}$. The magnitude uncertainty, in hundredths of a magnitude, has the same notation as the velocity width uncertainty in Col. 12.
Col. 16: If an asterisk appears in this column, special comments on the object are available in section 3.5.

Figure 2 (upper panels) shows the spatial distribution of the galaxies in the A2634 and Coma TF samples (large filled and open symbols identify proper and peripheral cluster members, respectively). The two dashed concentric circles have respectively radii of 1 and 2 Abell radii, R_A. In the lower panels of Figure 2, the radial velocity is plotted versus the angular separation from the cluster center; the dashed vertical lines are at 1 and 2 R_A, the solid horizontal lines refer to the systemic velocity of the two clusters, and the solid curves mark the redshift space caustic lines, taken from S95 for A2634 and from Regös & Geller (1989) for Coma. In both panels the small filled symbols indicate other galaxies with measured redshift located in the area.

The galaxies in the FP samples of A2634 and Coma are listed in Tables 3 and 4, respectively. The spectroscopic observations of the 109 Coma galaxies in Table 4 derive principally from a large extant body of data, namely: 51 objects from Lucey *et al.* (1991b, hereafter L91b), 36 S0 galaxies from Dressler (1987), and 37 E galaxies jointly from Davies *et al.* (1987) and Faber *et al.* (1987). The spectroscopy of the 55 galaxies listed in Table 3, in the cluster A2634, includes our own observations, complemented by 18 objects in the L91a sample. This sample of 55 objects includes

3 possible members of the foreground group near 7,000 $\mathrm{km\,s^{-1}}$ and one in the background group near 11,000 $\mathrm{km\,s^{-1}}$ discussed by S95. All the photometric data in tables 3 and 4 are new and obtained by us. The contents of Tables 3 and 4 are organized as follows:
Col. 1: Galaxy name, using one or two galaxy identifiers, as in Table 2. For Coma, the second identifier lists the Dressler (1980) catalog number (in the format Dnnn) for galaxies that are not included either in the NGC/IC or the CGCG.
Cols. 2 and 3: Right Ascension and Declination, in 1950.0 epoch.
Col. 4: Morphological type code, in the RC3 scheme (-5 for E, -2 for S0, 0 for S0a). Morphological types were derived from visual inspection of the blue plates of the POSS. Few objects originally classified as S0 had their type revised to Sa after inspection of the CCD images
Col. 5: Measured apparent I band magnitude.
Col. 6: Radial velocity, in $\mathrm{km\,s^{-1}}$, measured in the CMB reference frame.
Col. 7: Angular distance from the cluster center, in degrees.
Col. 8: Measured effective radius, in arcseconds.
Col. 9: Effective radius, in arcseconds, corrected for seeing effects. This is done adopting the prescriptions of Saglia *et al.* (1993, see in particular their figure 8).
Col. 10: Uncertainty on the effective radius, in arcseconds.
Col. 11: Corrected metric effective radius, in kiloparsec, obtained assuming the galaxy is at the distance indicated by the cluster redshift and $H_\circ = 100$ km s^{-1} Mpc^{-1}, in the CMB reference frame.
Col. 12: Measured effective surface brightness, in I band magnitudes per square arcsecond.
Col. 13: Corrected effective surface brightness, in I band magnitudes per square arcsecond. We corrected μ_e for the smearing effects of seeing, adopting the prescriptions of Saglia *et al.* (1993, see in particular their figure 8), for extinction within our Galaxy, using Burstein & Heiles (1978) method as described above, for the cosmological k-correction term (which is simply $2.5\log(1+z)$ because of the flat spectrum of early type galaxies in the far red), and for the $(1+z)^4$ cosmological dimming.
Col. 14: Uncertainty on the effective surface brightness, in magnitudes per square arcsecond.
Col. 15: Stellar velocity dispersion, in $\mathrm{km\,s^{-1}}$. For our new measurements, the measurement uncertainty, in $\mathrm{km\,s^{-1}}$, is given between brackets: e.g. 177(11) is equivalent to 177 ± 11 $\mathrm{km\,s^{-1}}$. Measurements taken from the literature are given without uncertainty. See original sources for details.
Col. 16: Reference codes for the spectroscopic measurements taken from the literature. If an asterisk appears in this column, special comments on the object are available in section 3.5 Whenever multiple spectroscopic measurements were available, we have used here only the one with smaller uncertainty. Therefore, if no reference is listed in col. 16, the new measurement presented in col. 15 was used for that particular galaxy. Otherwise, the measurement in the referenced source, and only that one, was used.

Figure 3 shows the spatial distribution (upper panels) and the radial velocity distribution as a function of angular distance from the cluster center (lower panels) for the A2634 and Coma FP

samples. Symbol and inset curves follow the same conventions as assumed for Figure 2.

4. Completeness corrections

It has been argued that cluster samples for TF and FP work are almost bias-free, since all galaxies are roughly at the same distance. While it is certainly true that the classical Malmquist bias is avoided, a different and equally important bias affects cluster samples. This is generally referred-to as the "cluster population incompleteness bias" (Teerikorpi 1987, 1990). In a recent work Sandage, Tammann & Federspiel (1995) have provided a detailed analysis of this bias and of the corrections it requires before unbiased distance estimates can be obtained with cluster TF samples. Their recipes are based on the assumption that galaxy samples are magnitude-limited. Since that is not the case for our samples, we have derived incompleteness bias corrections following the spirit of the Sandage *et al.* (1995) treatment, but using Monte Carlo simulations to reproduce as closely as possible the completeness, measurement uncertainties, and scatter characteristic of our samples. We refer the reader to the discussion in G96b for the details on the bias correction applied to the TF samples, while here we discuss briefly the bias correction for the FP samples, since the latter is derived using a significantly different procedure (a more detailed discussion will be given in Scodeggio 1997).

It is customary to express the completeness of a sample relatively to the expected luminosity distribution of a galaxy population, mainly because magnitudes are relatively easy to measure, and sample selection most often is based on them. We therefore define completeness as the ratio of the number of galaxies of a given magnitude included in a sample with respect to the total number of galaxies of the same magnitude predicted by the appropriate luminosity function.

The effect of sample incompleteness on the TF relation is relatively straightforward, because magnitude is one of the two parameters used to build the relation. At any given velocity width, fainter galaxies are preferentially missing from an incomplete sample, and this affects the determination of the slope, the zero-point, and the dispersion of the TF relation. In the FP case, magnitudes enter only indirectly into the FP diagram, via the existing relations between luminosity and effective radius (Fish 1964), velocity dispersion (Faber & Jackson 1976), and effective surface brightness (Binggeli, Sandage & Tarenghi 1984). These $L - R_e$, $L - \sigma$, and $L - \mu_e$ relations all show rather large scatter. Therefore, at any given velocity dispersion or effective surface brightness, the systematic lack of fainter galaxies is only marginally reflected into a lack of small effective radius objects, and it is not possible to translate the completeness of a sample directly in terms of an effective radius, velocity dispersion or effective surface brightness completeness. Our simulations are therefore designed to reproduce as closely as possible the observed relations between R_e and σ and the galaxy luminosity, and the relation between R_e and μ_e (Kormendy 1977). Then we select galaxies according to their magnitude, reproducing the observed luminosity incompleteness, and measure the indirect effect of this incompleteness on the FP parameters. In practice, we first divide both a complete sample and an incomplete one into bins according to the value of

the combination of σ and μ_e that provides an edge-on view of the fundamental plane. Then we measure the mean value of R_e for each bin, and compare these mean values for the complete and incomplete samples. Because of the lack of low luminosity objects, the mean R_e measured in the incomplete sample is systematically larger than the one measured for the complete sample, except in the two to three bins which include the most luminous galaxies. We finally use these differences to correct the observed values of R_e, and reproduce a relation as close as possible to the unbiased one.

5. The Relative Distance between Coma and A2634

5.1. TF

Although the results of S95 revealed that the A86 result was unlikely to be severely affected by substructure in A2634, the A86 TF sample was quite small and sparse. The situation improved with the study of G96a, which included a sample of 15 strict members and two additional cluster outliers. Our current sample includes 23 *bona fide* cluster members, and 4 peripheral members, nearly tripling the size of the A86 sample. The TF relation for our new data is shown in Figure 4a. Filled symbols indicate cluster members, and unfilled ones indicate peripheral members. The solid line is the TF template derived by G96b combining a sample of 555 galaxies in 24 clusters:

$$M_I = -21.00(\pm 0.02) - 7.76(\pm 0.13)\log(W - 2.5) \quad (1)$$

The total uncertainty in the TF template zero point is 0.05 mag. This includes statistical uncertainties associated with the fit (0.02 mag), uncertainties associated with the incompleteness bias corrections (0.025 mag), which are related to the choice of parameters that describe the luminosity function of spiral galaxies, and the estimated accuracy to within which the average peculiar velocity of the cluster set approaches zero in the CMB reference frame (0.04 mag). An uncertainty of 0.05 mag translates to about 210 $\mathrm{km\,s^{-1}}$ at the distance of A2634, and 170 $\mathrm{km\,s^{-1}}$ at the distance of Coma. The mean scatter about the TF template relation is $\simeq$0.35 mag., although this figure varies with the mean velocity width (and luminosity) of galaxies: it reduces to $\simeq$0.25 mag. at the high $\log W$ end, and expands to $\simeq$0.45 mag. at the low $\log W$ end of the typical range of the TF diagram.

The mean offset from the template, for the A2634 sample shown in Fig. 4a, is –0.04±0.06 mag., corresponding to a peculiar velocity of +165±250 $\mathrm{km\,s^{-1}}$ in the CMB reference frame. For comparison, the peculiar velocity estimate obtained by G96b using only 15 strict cluster members is +61±378 $\mathrm{km\,s^{-1}}$.

For later comparison with the FP results, we also derive a Coma-A2634 relative TF distance. Figure 4b shows the TF relation for the Coma sample of G96a. The convention for the symbols and the solid line are the same as in Fig. 4a. The mean offset from the template for Coma is –0.06±0.06 mag., corresponding to a peculiar velocity of +194±196 $\mathrm{km\,s^{-1}}$. The relative

peculiar motion of A2634 with respect to Coma is therefore -29±318 $\mathrm{km\,s^{-1}}$, and the ratio of their distances is 1.25 ± 0.03. We remark also that the differential bias correction between the two clusters is only 0.002 magnitudes, and therefore the amplitude of the Coma–A2634 relative motion in the comoving frame is practically independent of the amplitude of the two separate bias corrections. In the comoving reference frame, it thus appear that the two clusters are at rest with respect to each other, as nearly determined as the error budget allows. The peculiar velocities of each of the two clusters also appear to be of statistically negligible amplitude.

5.2. FP

The $\mathrm{D_n} - \sigma$ and FP relations have been obtained in the past using photometric measurements in many different bands, from B (Faber *et al.* 1989) to V (L91a, L91b), r_G (Djorgovski & Davis 1987), Gunn r (Jørgensen, Franx & Kjærgaard 1996), and Kron-Cousins R (Colless *et al.* 1993). In the study of early-type galaxies there are no compelling reasons for favoring one optical band over the others. Our adoption of I band for photometry was mainly dictated by the practical notion that the cluster images contain several galaxies per frame, both of early– and late–type, and thus can be useful for TF application, where the I band is favored for compatibility with G96a.

The FP is a flat surface in the 3-dimensional space of the parameters $\log R_e$, $\log \sigma$, and μ_e. We use the data set of 109 Coma galaxies listed in Table 4 in order to obtain a FP template relation, which we define as the plane obtained by averaging the coefficients of the 3 possible fits that can be performed using one of the 3 parameters as the dependent variable and the remaining two as the independent ones. The resulting FP template, obtained by assuming that Coma is at rest in the CMB reference frame and $\mathrm{H_\circ} = 100$ km s^{-1} Mpc^{-1}, is given by

$$\log R_e = 1.25(\pm 0.021) \log \sigma + 0.32(\pm 0.012)\ \mu_e - 8.38(\pm 0.008) \qquad (2)$$

(or $\log R_e = 1.25 \log \sigma - 0.79 \log I_e - 8.38$). No statistically significant difference is observed when only E or only S0 galaxies are considered. The dispersion around this mean relation, measured as the r.m.s. scatter in the residuals of $\log R_e$, is 0.086. This is in remarkable agreement with the result of Jørgensen, Franx & Kjærgaard (1996), who found a scatter in $\log R_e$ of 0.084. The dispersion is equivalent to a scatter of 0.43 mag in the distance modulus (or 20% in distance) of a single galaxy. The statistical uncertainty on the FP zero point is of 0.008, equivalent to a distance (or peculiar velocity) uncertainty for the Coma cluster of 133 $\mathrm{km\,s^{-1}}$. The incompleteness bias correction for this sample was derived fitting a Fermi-Dirac distribution to the completeness histogram. The 50% completeness level is at $M_I = -20.20$, while the mean I band magnitude of a complete sample is $\simeq -20.65$. The mean bias correction to $\log R_e$ derived from the Monte Carlo simulations is 0.018 (equivalent to a correction of 0.090 mag for the distance modulus).

Figure 5 shows an edge-on view of the FP for the Coma sample. The solid line is the projection of the plane (2). To make the figure more readable we plot separately the data points and the error-bars associated with those points. As already pointed out by Djorgovski & Davis

(1987), and Jørgensen, Franx & Kjærgaard (1996), there might be a small curvature in the plane. Galaxies with the smallest and largest effective radii appear to have systematically positive residuals in $\log R_e$, but the number of objects involved is too small to make this effect statistically significant.

Figure 6 shows the edge-on view of the FP for the A2634 sample. The solid line is the FP template derived for Coma. Error-bars are plotted separately in panel (b). Two galaxies in this sample deviate significantly ($> 4\sigma$) from the main relation. One (330747) is a small companion to a much brighter galaxy (UGC 12727), so that the iterative subtraction procedure used to obtain its photometric parameters yields uncertain results. The second galaxy (331345) has a very flat photometric profile, with abnormally faint central surface brightness (its effective surface brightness is almost a magnitude fainter than the next fainter effective surface brightness in our sample). We have excluded these two galaxies from the A2634 sample used to derive the cluster peculiar motion.

The relative agreement between data-points and template line seen in Figure 6 indicates that the difference in peculiar velocity between Coma and A2634 is small. The mean offset in $\log R_e$ between A2634 and the Coma template (2) is -0.01±0.013, which corresponds to a peculiar velocity of –204±266 $\mathrm{km\,s^{-1}}$ for A2634, with respect to Coma in the comoving reference frame. The ratio of the distances of the two clusters, according to this FP analysis, is 1.27 ± 0.03 This result is in good agreement with the estimates obtained using the completely independent spiral samples and the TF relation, and in disagreement with the result of L91a. The A2634 sample is characterized by a 50% completeness level at $M_I = -20.70$, and by a bias correction of 0.021 dex. The differential bias correction between Coma and A2634 is therefore only 0.003 dex (equivalent to 0.015 magnitudes on the distance modulus), and does not play a significant role in the determination of the relative motion between the two clusters.

In order to identify the source of the discrepancy with the results of L91a, we have re-determined the A2634 peculiar velocity using two subsets of our sample.

The first subset is composed of the 18 galaxies observed by L91a. For this computation we used our own I band photometric measurements, and the original velocity dispersion measurements of L91a. The mean residual in $\log R_e$ for this sample is -0.070±0.028, corresponding to a peculiar velocity of –1324±573 $\mathrm{km\,s^{-1}}$. This is significantly bigger than the value we obtain using the whole sample, but also smaller than the value obtained by L91a using the same velocity dispersions, and their own photometric measurements. As discussed in § 3.3, from a direct comparison of velocity dispersions the L91a measurements appear to be systematically larger, by $\simeq$14%, than our measurements, but this difference alone is not enough to explain the discrepancy between our distance estimate for A2634 and the L91a one. Unfortunately L91a published only V band isophotal diameters for their galaxies, and a comparison with our I band photometry for those same galaxies is very difficult, without accurate V-I color information. Therefore we hesitate to carry the analysis of the L91a sample any further.

We repeat the exercise with a second A2634 subset, composed of the 42 galaxies for which we have obtained both photometric and spectroscopic measurements (but two galaxies are removed from the sample, as discussed above). The mean residual in $\log R_e$ for this sample is 0.000±0.014, which corresponds to a relative peculiar velocity of 0±287 $\mathrm{km\,s^{-1}}$. The result is again in good agreement with the TF determination.

The small uncertainties in the TF and FP determinations we have just discussed, and the good agreement between the two independent results, indicate that the peculiar velocity of A2634 is small. We conclude that the L91a result is spurious and find no reason to doubt that the FP and TF relations have universal applicability. Similar conclusions have been recently obtained by Lucey and coworkers, using new velocity dispersion measurements in A2634 and A2199 (Guzman 1996). These new measurements confirm that the measurements reported by L91a were systematically overestimated, and therefore that the peculiar velocity of A2634 is negligible.

6. Conclusions

New TF and FP measurements for the cluster A2634 and Coma give compatible results for the relative distance and peculiar velocity of the two clusters. Contrary to the findings of L91a, the peculiar velocity of A2634 with respect to the CMB reference frame is unlikely to exceed a few 10^2 $\mathrm{km\,s^{-1}}$, and extremely unlikely to exceed 10^3 $\mathrm{km\,s^{-1}}$.

Both TF and FP measurements suggest that the ratio of the distances to A2634 and to Coma is $\sim 1.26 \pm 0.03$, which is not too dissimilar from the ratio of systemic velocities in the CMB reference frame of 1.24. Our determinations are more accurate and reliable than those of previous work, thanks to (a) more accurate criteria for the assignment of cluster membership to individual galaxies and (b) significantly expanded samples.

We have also obtained a new FP template, using for the first time I band photometry. The parameters of this template are in very good agreement with recent determinations of the FP obtained at shorter wavelengths (Gunn r), confirming that there is little dependence of the FP relation on the passband used for the photometric measurements. The uncertainty with which the FP can provide peculiar velocity estimates for single galaxies is $\simeq$0.43 mag in the distance modulus, or 20% of the distance. This uncertainty is slightly larger than the typical uncertainty that characterizes TF estimates, the latter being $\simeq$0.35 magnitudes. This disadvantage is however partly compensated by the fact that the sample incompleteness bias has a less severe effect on FP cluster distance estimates than it has on TF cluster distance estimates, and cluster membership is more readily established for early–type objects.

The original motivation for this study was provided by the desire to investigate the universality of the TF and FP relations, the discrepancy in peculiar velocity estimates reported by L91a making A2634 an extreme case study. Our results restore a measure of trust in the reliability of those relations as cosmological tools.

We would like to thank Juan Carrasco for the precious help he provided during the observing runs at Palomar, and Bill Schoening for his assistance with the 0.9m telescope at KPNO. We are grateful to the KPNO TAC for the generous allocation of observing time. This research was partially supported by NSF grants AST94–20505 to RG, and AST90–23450 and AST92–18038 to MPH.

A. Comments on individual objects: A2634

330564: marginal cluster membership assignment.
331234: probably a member of an interacting system.
330636: extremely irregular system, with several clumps of light spread in irregular fashion. Inclination unreliable.
330663: spectrum with poor s/n ratio; very uncertain width.
U12721: the discrepancy in flux among multiple sources reported by G96a is resolved by these observations.
U12755: the magnitude reported by G96a is 12.43; new observations yield 12.46; we adopt the average value.

U12716: σ measured also by L91a (327 $\mathrm{km\,s^{-1}}$), Tonry 1984 (348 $\mathrm{km\,s^{-1}}$), Malumuth & Kirshner 1981 (386 $\mathrm{km\,s^{-1}}$), Tonry & Davis 1981 (365 $\mathrm{km\,s^{-1}}$), and Faber *et al.* 1989 (298 $\mathrm{km\,s^{-1}}$).
331456: σ measured also by L91a (218 $\mathrm{km\,s^{-1}}$), and by Tonry 1984 (250 $\mathrm{km\,s^{-1}}$).
330649: σ measured also by L91a (285 $\mathrm{km\,s^{-1}}$).
330658: σ measured also by L91a (201 $\mathrm{km\,s^{-1}}$).
330668: σ measured also by L91a (207 $\mathrm{km\,s^{-1}}$).
330678: σ measured also by L91a (272 $\mathrm{km\,s^{-1}}$).
331456, 330648, 330651, 330658, 330660, 330665, 330668, 330678 are within the halo of the cD UGC 12716; their μ_e has high uncertainty.
330706: bright nearby star subtracted.
330600: faint outer disk visible.
330747: bright nearby companion (UGC 12727) subtracted. Surface brightness determination unreliable.
U12744: bright nearby star subtracted.

B. Comments on individual objects: Coma

U8049: σ also measured by L91b (212 $\mathrm{km\,s^{-1}}$), and Faber *et al.* 1989 (208 $\mathrm{km\,s^{-1}}$).
U8065: σ also measured by L91b (279 $\mathrm{km\,s^{-1}}$).
U8070: σ also measured by Davies & Illingworth 1983 (255 $\mathrm{km\,s^{-1}}$), Faber *et al.* 1989 (259 $\mathrm{km\,s^{-1}}$), and L91b (298 $\mathrm{km\,s^{-1}}$).

U8103: σ also measured by L91b (279 $\mathrm{km\,s^{-1}}$), Faber *et al.* 1989 (245 $\mathrm{km\,s^{-1}}$), Malumuth & Kirshner 1981 (304 $\mathrm{km\,s^{-1}}$). Ours spectrum has poor s/n ratio, and therefore we use Faber *et al.* measurement.
U8110: σ also measured by Oegerle & Hoessel 1991 (381 $\mathrm{km\,s^{-1}}$), Tonry 1985 (404 $\mathrm{km\,s^{-1}}$), Tonry & Davis 1981 (412 $\mathrm{km\,s^{-1}}$), Davies & Illingworth 1983 (342 $\mathrm{km\,s^{-1}}$), Faber *et al.* 1989 (381 $\mathrm{km\,s^{-1}}$), Faber & Jackson 1976 (400 $\mathrm{km\,s^{-1}}$), and L91b (414 $\mathrm{km\,s^{-1}}$).
U8175: σ also measured by L91b (275 $\mathrm{km\,s^{-1}}$).
221266: σ also measured by Davies *et al.* 1987 (150 $\mathrm{km\,s^{-1}}$).
221354: σ also measured by L91b (147 $\mathrm{km\,s^{-1}}$), and Faber et al. 1989 (164 $\mathrm{km\,s^{-1}}$).
221410: σ also measured by Dressler 1987 (133 $\mathrm{km\,s^{-1}}$).
221216: spectrum with poor s/n ratio. Also, the galaxy is in a close pair.
221290, 221291, 221293, 221298, 221303, 221304, 221317, 221323, 221329, 221331, 221334 are within the halo of the D galaxy UGC 8103, and 221354, 221362, 221377, 221380, 221382, 221392 are within the halo of the D galaxy UGC 8110; their μ_e has high uncertainty.
U8133: faint outer disk.
U8072/U8073: close pair; iterative subtraction required.
U8100: bright nearby star subtracted.

REFERENCES

Aaronson, M., Bothun, G., Mould, J., Huchra, J., Schommer, R.A., & Cornell, M.E. 1986, ApJ, 302, 536 (A86)

Bender, R. 1990, A&A, 229, 441

Binggeli, B., Sandage, A., & Tarenghi, M. 1984, AJ, 89, 64

Burstein, D. & Heiles, C. 1978, ApJ, 225, 40

Colless, M., Burstein, D., Wegner, G., Saglia, R.P., McMahan, R., Davies, R.L., Bertschinger, E., & Baggley G. 1993, MNRAS, 262, 475

Colless, M., & Dunn, A.M. 1996, ApJ, 458, 435

David, L.P., Slyz, A., Jones, C., Forman, W., Vrtilek, S.D., & Arnaud, K.A. 1993, ApJ, 412, 479

Davies, R.L., & Illingworth, G. 1983, ApJ, 266, 516

Davies, R.L., Burstein, D., Dressler, A., Faber, S.M., Lynden-Bell, D., Terlevich, R.J., & Wegner, G. 1987, ApJS, 64, 581

Djorgovski, S., & Davis, M. 1987, ApJ, 313, 59

Djorgovski, S., De Carvalho, R., & Han, M.S. 1988, in "The Extragalactic Distance Scale", ed. S. van den Bergh & J. Pritchet, p. 329

Dressler, A. 1980, ApJ, 236, 351

Dressler, A. 1987, ApJ, 317, 1

Dressler, A., Lynden-Bell, D., Burstein, D., Davies, R.L., Faber, S.M., Terlevich, R.J., & Wegner, G. 1987, ApJ, 313, 42

Faber, S.M., & Jackson R.E. 1976, ApJ, 204, 668

Faber, S.M., Wegner, G., Burstein, D., Davies, R.L., Dressler, A., Lynden-Bell, D., & Terlevich, R.J., & 1987, ApJS, 69, 763

Fish, R.A. 1964, ApJ, 139, 284

Franx, M. 1993, PASP, 105, 1058

Franx, M., Illingworth, G., & Hechman, T. 1989, ApJ, 344, 613

Gavazzi, G., Randone, I., & Branchini, E. 1995, ApJ, 438, 590

Giovanelli, R., & Haynes, M.P. 1989, AJ, 97, 633

Giovanelli, R., & Haynes, M.P. 1991, ARA&A, 29, 499

Giovanelli, R., Haynes, M.P., Salzer, J.J., Wegner, G., da Costa, L.N., & Freudling, W. 1995, AJ, 110, 1059

Giovanelli, R., Haynes, M.P., Herter, T., Vogt, N.P., Wegner, G., Salzer, J.J., da Costa, L.N. and Freudling, W., 1996a, AJ submitted (G96a)

Giovanelli, R., Haynes, M.P., Herter, T., Vogt, N.P., da Costa, L.N., Freudling, W., Salzer, J.J. and Wegner, G., 1996b, AJ submitted (G96b)

Guzmán, R. 1996, private communication

Guzmán, R., Lucey, J.R., Carter, D., & Terlevich, R.J. 1992, MNRAS, 257, 187

Han, M.S. 1992, ApJS, 81, 35

Jacoby, G.H., Branch, D., Ciardullo, R., Davies, R.L., Harris, W.E., Pierce, M.J., Pritchet, C.J., Tonry, J.L., & Welch, D.L. 1992, PASP, 104, 599

Jørgensen, I., Franx, M., & Kjærgaard, P. 1996, MNRAS, 280, 167

Kent, S.M., & Gunn, J.E. 1982, AJ, 87, 945

Kogut, A., et al. 1993, ApJ, 419, 1

Kormendy, J. 1977, ApJ, 218, 333

Landolt, A.U. 1992, AJ, 104, 340

Lynden-Bell, D., Faber, S.M., Burstein, D., Davies, R.L., Dressler, A., Terlevich, R.J., & Wegner, G. 1988, ApJ, 326, 19

Lucey, J.R., Gray, P.M., Carter, D., & Terlevich, R.J. 1991a, MNRAS, 248, 804 (L91a)

Lucey, J.R., Guzmán, R., Carter, D., & Terlevich, R.J. 1991b, MNRAS, 253, 584 (L91b)

Malumuth, E.M., & Kirshner, R.P. 1981, ApJ, 251, 508

Mould, J.R., et al. 1990, ApJ, 383, 467

Oegerle, W.R., & Hoessel, J.G. 1991, ApJ, 375, 15

Oke, J.B., & Gunn, J.E. 1982, PASP, 94, 586

Pinkney, J., Rhee, G., Burns. J.O., Hill, J.M., Oegerle, W.M., Batuski, D., & Hintzen, P. 1993, ApJ, 416, 36

Regös, E., & Geller, M.J. 1989, AJ, 98, 755

Rowan-Robinson, M. 1985, "The Cosmological Distance Ladder" (New York, Freeman and Co.)

Saglia, R.P. Bertschinger, E., Baggley, G., Burstein, D., Colless, M., Davies, R.L., McMahan, R.K., & Wegner, G. 1993, MNRAS, 264, 961

Sandage, A. 1994a, ApJ, 430, 1

Sandage, A. 1994b, ApJ, 430, 13

Sandage, A., Tammann, G.A., & Federspiel, M. 1995, ApJ, 452, 1

Sargent, W.L.W., Schechter, P.L., Boksenberg, A., & Shortridge, K. 1977, ApJ, 212, 326

Scodeggio, M. 1997, Ph. D. Thesis, Cornell University

Scodeggio, M., Solanes, J.M., Giovanelli, R., & Haynes, M.P. 1995, ApJ, 444, 41 (S95)

Scodeggio, M., Giovanelli, R., & Haynes, M.P. 1996, in preparation

Silk, J. 1989, ApJ, 345, L1

Teerikorpi, P. 1984, A&A, 141, 407

Teerikorpi, P. 1987, A&A, 173, 39

Teerikorpi, P. 1990, A&A, 234, 1

Teerikorpi, P. 1993, A&A, 280, 443

Tonry, J.L. 1984, ApJ, 279, 13

Tonry, J.L. 1985, AJ, 90, 2431

Tonry, J.L., & Davis, M. 1979, AJ, 84, 1511

Tonry, J.L., & Davis, M. 1981, ApJ, 246, 666

Tully, R.B., & Fisher, J.R. 1977, A&A, 54, 661

van Dokkum, P.G., & Franx, M. 1996, MNRAS, 281, 985

Vogt, N.P., Herter, T., Haynes, M.P., & Courteau, S. 1993, ApJ, 415, L95

Vogt, N.P., Forbes, D.A., Phillips, A.C., Gronwall, C., Faber, S.M., Illingworth, G.D., & Koo, D.C. 1996, ApJ, 465, L15

Willick, J.A. 1994, ApJS, 92, 1

Zabludoff, A.I., Huchra, J.P., & Geller, M.J. 1990, ApJS, 74, 1

Fig. 1.— Comparison of our velocity dispersion measurements with literature data. The difference (our – literature) is plotted vs. our measurements. Filled symbols: Coma cluster galaxies, with measurements from L91b, Davies *et al.* (1987), and Faber *et al.* (1987). Empty symbols: A2634 galaxies, with measurements from L91a. The lines connecting pairs of data-points identify 3 galaxies for which multiple comparisons are available.

Fig. 2.— Spatial distribution (upper panels) and cz_{CMB} vs. angular separation from the cluster center (lower panels) for the A2634 and Coma TF samples. Filled circles indicate galaxies that are considered cluster members; empty circles indicate peripheral cluster member; asterisks indicate members of foreground or background groups (see discussion in the text). Small symbols indicate all galaxies with measured redshift located in the area. The two dashed circles (upper panels), and the two dashed vertical lines (lower panels) refer to distances of 1 and 2 R_A from the cluster centers. The horizontal lines in the lower panels mark the cluster systemic velocity in the CMB reference frame. The curved solid lines are the redshift-space caustic lines estimated for $\Omega_\circ = 0.3$.

Fig. 3.— FP samples, plotted in the same mode and convention as described for figure 1.

Fig. 4.— (a) TF diagram for A2634. (b) TF diagram for Coma. In both figures filled and empty symbols indicate cluster members and peripheral members, respectively. The solid line is the G96b TF template (equation 1).

Fig. 5.— Edge-on view of the FP for Coma. The upper panel shows the data points, and the projection of the best fitting plane (equation 2). The lower panel shows the error bars associated with the upper panel data points.

Fig. 6.— Edge-on view of the FP for A2634. The inset straight line is the FP template relation computed for the Coma sample. Filled and empty symbols indicate cluster members and peripheral members, respectively, and asterisks indicate the possible members of foreground and background groups (see discussion in the text).

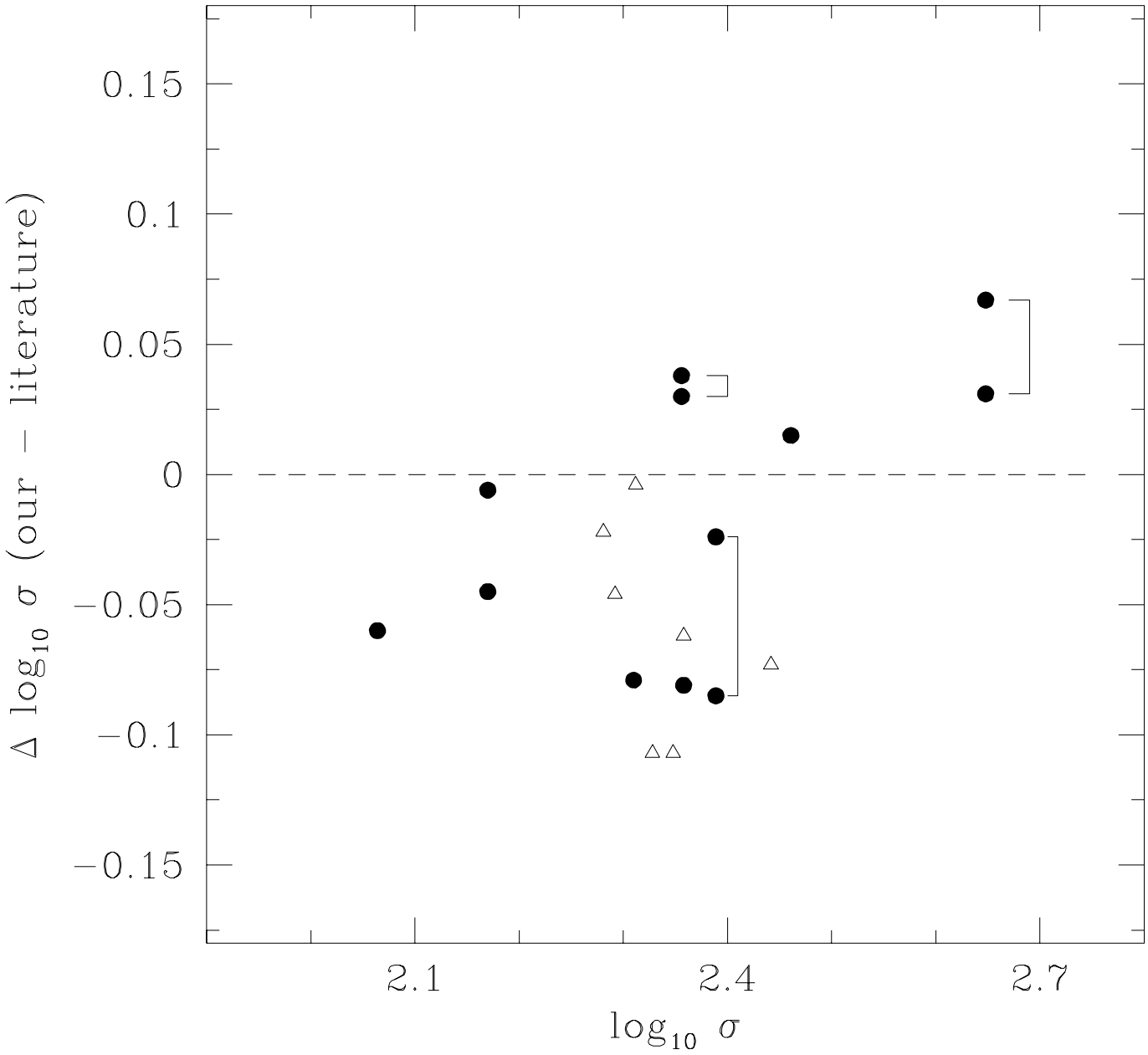
0.15
0.1
0.05
0
−0.05
−0.1
−0.15
Δ log10 σ (our − literature)
2.1
2.4
2.7
log10 σ

TABLE 1. Clusters parameters

	A2634	Coma	ref.
Cluster center (1950)	23 35 54.9 26 44 19	12 57 11.1 28 13 48	
V_{hel} ($km\,s^{-1}$)	9240	6917	1
V_{CMB} ($km\,s^{-1}$)	8895	7185	1
Vel. disp ($km\,s^{-1}$)	661	1010	1
R_A (deg.)	0.96	1.19	
L_x(2-10 kev) (erg s^{-1})	5.22 10^{43}	6.02 10^{44}	2
T (kev)	3.4	8.3	2
Spiral fraction (%)	36	15	3

References for Table 1.

1: Scodeggio et al. 1995 (A2634); Zabludoff, Geller & Huchra 1990 (Coma)
2: David et al. 1993
3: Dressler 1980

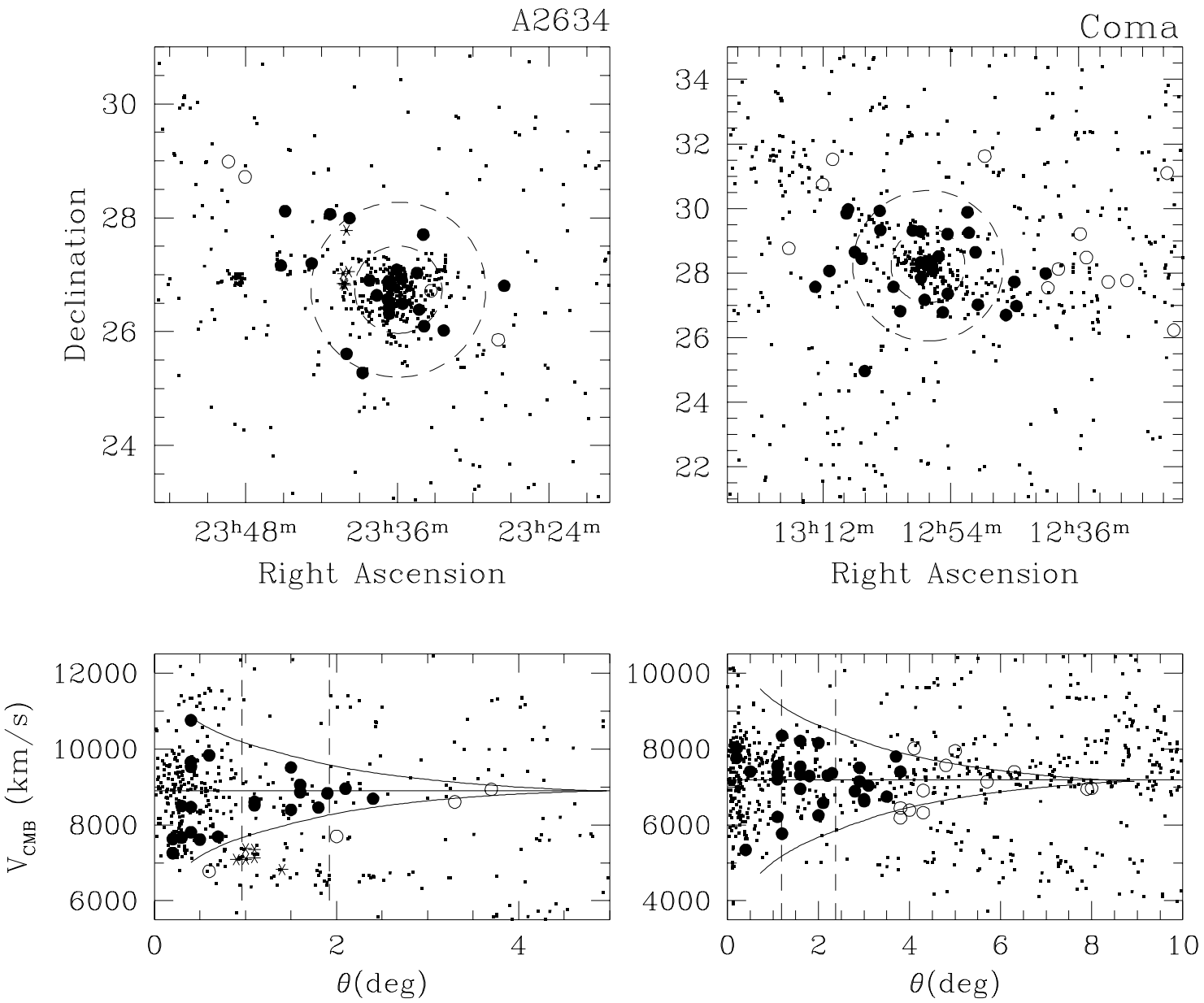
A2634
Coma
Declination
30
28
26
24
34
32
30
28
26
24
22
23h48m
23h36m
23h24m
13h12m
12h54m
12h36m
Right Ascension
Right Ascension
V_CMB (km/s)
12000
10000
8000
6000
10000
8000
6000
4000
0
2
4
0
2
4
6
8
10
θ(deg)
θ(deg)

TABLE 2. Galaxy TF Parameters: A2634

Names	R.A.	Dec.	T	V_{cmb}	θ	gr	W	W_1	W_{cor}	i	log W_{cor}	m	m_{cor}	M_{cor}	Notes
	(1950)	(1950)		km s^{-1}	deg		—	km s^{-1}	—	deg		mag	mag	mag	
(1)	(2)	(3)	(4)	(5)	(6)	(7)	(8)	(9)	(10)	(11)	(12)	(13)	(14)	(15)	(16)
U12631/476-054	23 27 32.5	26 48 20	3	8833	1.9	c	466	433	451	74	2.654(06)	13.07	12.77	-22.01(11)	
331192	23 28 01.1	25 51 29	5	7697	2.0	g	259	231	261	62	2.417(69)	14.28	13.94	-20.52(05)	
U12678/476-072	23 32 20.0	26 01 13	3	8608	1.1	c	516	471	471	90	2.673(09)	13.31	12.64	-22.14(17)	
330564	23 33 19.9	26 43 07	3	6779	0.6	g	302	302	332	66	2.520(20)	13.44	13.17	-21.61(08)	*
331230	23 33 53.1	26 05 49	3	7691	0.7	c	241	208	238	61	2.376(25)	15.18	14.90	-19.89(12)	
U12701	23 33 56.6	27 42 17	5	8512	1.1	c	379	323	330	79	2.518(17)	14.39	13.79	-21.00(11)	
331234	23 34 16.2	26 23 09	3	8468	0.4	c	155	125	146	59	2.163(47)	16.09	15.88	-18.90(11)	*
330581	23 34 26.4	27 01 46	3	9524	0.4	c	269	283	295	74	2.469(15)	14.90	14.48	-20.30(09)	
330633	23 35 34.6	26 29 33	5	8405	0.3	c	356	326	333	78	2.522(10)	14.47	13.88	-20.90(09)	
330636	23 35 39.7	26 55 28	10	7625	0.2	c	131	111	117	71	2.067(132)	15.95	15.59	-19.18(12)	*
330663	23 36 02.5	27 05 17	3	9662	0.4	c	273	227	227	90	2.356(54)	15.26	14.60	-20.18(20)	*
330714	23 36 39.0	26 18 40	10	7611	0.5	c	156	133	138	74	2.141(47)	16.54	16.15	-18.63(11)	
330718	23 36 39.3	26 24 58	5	7803	0.4	c	211	185	191	75	2.281(16)	15.95	15.46	-19.32(08)	
U12721/476-098	23 36 41.4	26 50 17	3B	7258	0.2	c	405	376	418	64	2.621(25)	12.74	12.47	-22.31(05)	*
330721	23 36 41.5	26 52 58	3	7256	0.2	c	278	278	278	90	2.443(28)	14.49	13.81	-20.96(14)	
330726	23 36 46.5	26 34 02	3	7666	0.3	c	172	145	170	59	2.252(50)	15.32	15.12	-19.65(04)	
330751	23 37 37.2	26 38 19	3	10756	0.4	c	129	97	196	30	2.293(89)	14.81	14.69	-20.09(05)	
330761	23 38 11.8	26 54 01	1	9833	0.6	c	221	195	265	47	2.423(35)	14.30	14.11	-20.67(09)	
330768/476-112	23 38 45.0	25 16 30	3	9052	1.6	c	448	417	456	66	2.659(11)	12.99	12.77	-22.01(10)	
331287	23 39 46.7	27 59 39	7	8396	1.5	c	216	187	211	63	2.324(26)	14.88	14.52	-20.25(05)	
330778/476-116	23 39 51.5	27 03 17	3	7089	0.9	7	399	396	397	85	2.599(08)	13.73	13.20	-21.11(14)	
331095	23 40 00.1	27 46 45	5	6827	1.4	7	250	223	224	84	2.351(10)	14.30	13.56	-20.75(16)	
331292	23 40 00.5	25 36 39	5	9513	1.5	c	240	199	294	43	2.469(46)	15.16	14.94	-19.84(04)	
330779/476-117	23 40 07.4	26 48 50	5	7136	1.1	7	291	263	333	52	2.523(34)	13.31	13.08	-21.22(09)	
330781	23 40 11.0	26 50 40	5	7374	1.0	7	306	277	290	73	2.463(12)	14.13	13.61	-20.70(13)	
U12746/476-119	23 40 15.1	27 01 23	5	7093	1.0	7	456	425	427	84	2.631(06)	13.09	12.27	-22.04(17)	
331297	23 40 18.1	26 50 31	5	7352	1.1	7	240	205	208	80	2.318(55)	14.80	14.13	-20.23(16)	
U12755/498-004	23 41 18.5	28 03 50	3B	8459	1.8	c	508	471	538	61	2.730(14)	12.43	12.19	-22.59(09)	*
331322	23 42 45.2	27 12 01	5	8858	1.6	c	285	255	268	72	2.428(12)	14.22	13.67	-21.11(07)	
330918/498-012	23 44 52.4	28 06 59	4	8690	2.4	c	383	350	384	66	2.584(10)	13.23	12.93	-21.85(12)	
330923/477-006	23 45 12.3	27 09 42	5	8956	2.1	c	418	381	397	74	2.599(08)	13.59	13.21	-21.57(10)	
U12803/498-018	23 48 02.1	28 43 14	3	8604	3.3	g	489	445	576	51	2.760(37)	12.27	12.10	-22.60(09)	
U12817/498-019	23 49 20.3	28 59 16	3	8935	3.7	g	471	438	452	75	2.655(07)	13.46	13.15	-21.64(12)	

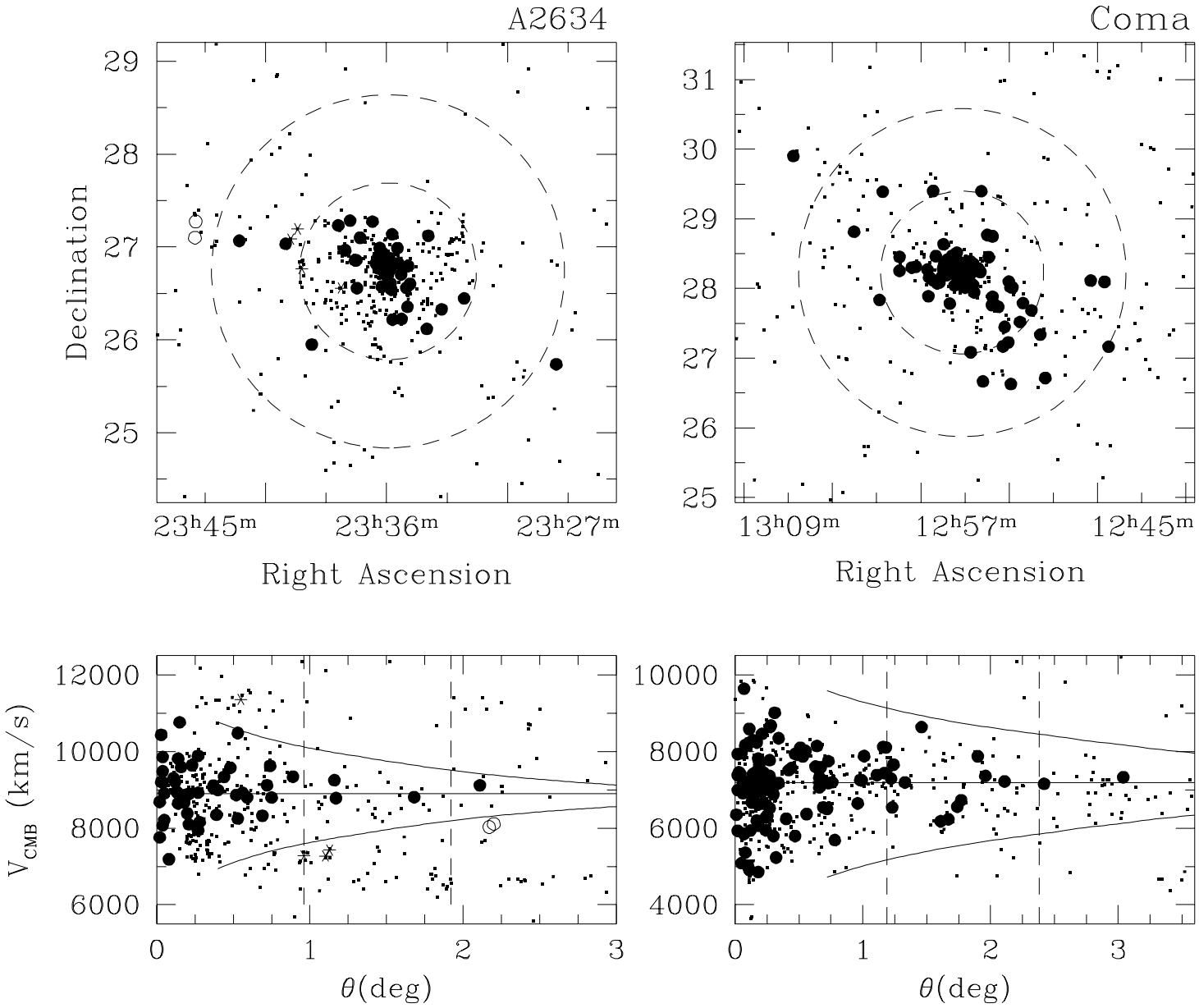
A2634
Coma
Declination
29
28
27
26
25
31
30
29
28
27
26
25
23h45m
23h36m
23h27m
13h09m
12h57m
12h45m
Right Ascension
Right Ascension
V_CMB (km/s)
12000
10000
8000
6000
10000
8000
6000
4000
0
1
2
3
θ(deg)
θ(deg)

TABLE 3. A2634 FP data

Names	RA	Dec	T	m	V_{CMB}	θ	r_e	r_e^c	ϵ_r	R_e	μ_e	μ_e^c	ϵ_μ	σ	ref.
	(1950)	(1950)		mag	km s^{-1}	deg	$''$	$''$	$''$	kpc	– mag/arcsec^2 –			km s^{-1}	
(1)	(2)	(3)	(4)	(5)	(6)	(7)	(8)	(9)	(10)	(11)	(12)	(13)	(14)	(15)	(16)
330499/476-052	23 27 34.8	25 44 14	-2	13.36	9117	2.1	5.89	5.68	0.17	2.45	18.92	18.60	0.040	177(11)	
330553/476-071	23 32 08.9	26 26 49	0	13.09	9342	0.9	10.20	10.06	0.35	4.34	19.52	19.25	0.043	192(12)	
331223	23 33 15.8	26 19 44	-5	14.29	9118	0.7	8.18	8.00	0.44	3.53	19.99	19.70	0.068	151(11)	
331231	23 33 56.0	27 07 17	-5	13.78	8801	0.6	13.60	13.49	0.53	5.82	20.12	19.86	0.045	165(11)	
331233	23 33 59.9	26 07 05	-5	13.99	8797	0.7	6.47	6.25	0.40	2.70	19.84	19.53	0.079	170(12)	
330595/476-079	23 34 49.9	26 36 04	-2	12.97	8156	0.3	10.47	10.31	0.43	4.45	19.56	19.31	0.050	199(12)	
330600	23 34 55.8	26 47 40	-2	13.71	9639	0.2	7.49	7.30	0.32	3.15	19.74	19.43	0.055	114(11)	*
330602	23 34 57.5	26 21 21	-2	14.19	9338	0.4	8.11	7.93	0.45	3.42	19.64	19.34	0.070	134(11)	
330604	23 35 01.3	26 33 37	-2	14.80	7947	0.3	2.66	2.26	0.16	0.97	18.60	18.04	0.088	167(13)	
330614/476-081	23 35 15.3	26 13 33	0	13.52	8248	0.5	30.79	30.79	1.71	13.28	21.05	20.82	0.057	159(11)	
330615	23 35 16.3	26 42 15	-2	13.83	10761	0.2	6.15	5.93	0.30	2.56	19.35	19.00	0.066	141	1
330621	23 35 25.1	26 49 26	0	14.26	9815	0.1	6.38	6.25	0.34	2.70	20.09	19.79	0.070	144	1
330624	23 35 27.6	26 59 14	-2	13.27	9886	0.3	7.13	6.91	0.31	2.98	19.35	19.03	0.057	169(11)	
331239	23 35 42.1	26 13 02	-5	13.58	8861	0.5	6.54	6.33	0.32	2.73	19.17	18.86	0.065	166(11)	
330643	23 35 43.4	27 08 13	-2	13.46	8992	0.4	5.80	5.55	0.24	2.39	18.49	18.16	0.057	199(13)	
330647/476-084	23 35 45.7	26 32 25	-2	14.10	8382	0.2	8.36	8.21	0.84	3.54	19.48	19.21	0.124	178(11)	
330649/476-085	23 35 48.1	26 36 35	-5	13.31	8951	0.1	4.92	4.76	0.14	2.05	18.67	18.36	0.041	223(11)	*
330648	23 35 48.2	26 45 30	-6	14.43	9207	0.0	2.28	2.02	0.12	0.87	18.01	17.50	0.100	182	1*
330651	23 35 50.3	26 46 27	0	14.05	9856	0.0	5.32	5.17	0.23	2.23	19.36	19.04	0.100	191	1*
330653/476-086	23 35 52.4	26 52 52	-5	13.22	8904	0.1	5.79	5.65	0.13	2.44	18.80	18.51	0.031	187(11)	
330658	23 35 56.5	26 42 29	-2	13.01	10434	0.0	7.31	7.18	0.19	3.10	19.39	19.09	0.100	191(11)	*
330659	23 35 56.7	26 48 49	-2	14.83	7187	0.1	33.11	33.11	3.11	14.28	21.69	21.48	0.085	98	1
330660/476-090	23 35 58.8	26 42 06	-5	12.87	9193	0.0	8.24	8.13	0.22	3.51	19.38	19.11	0.100	263	1*
U12716/N7720A	23 35 59.1	26 45 14	-4	10.31	8686	0.0	18.43	18.40	0.18	7.93	19.58	19.33	0.011	277(13)	*
331456/N7720B	23 35 59.2	26 45 26	-5	13.97	7759	0.0	3.36	3.17	0.10	1.37	17.85	17.48	0.100	196(13)	*
330665	23 36 02.9	26 45 29	-5	14.17	9483	0.0	3.71	3.53	0.16	1.52	18.68	18.32	0.100	173	1*
330667	23 36 04.1	26 42 09	-2	13.93	8211	0.1	1.89	1.57	0.08	0.68	16.80	16.19	0.062	236	1
330668/476-090B	23 36 05.9	26 45 09	-2	12.86	8074	0.0	13.74	13.67	0.59	5.90	20.15	19.91	0.100	205(12)	*
330678	23 36 08.0	26 44 00	-5	13.06	8907	0.1	5.82	5.68	0.13	2.45	18.78	18.48	0.100	213(11)	*
330679/476-095B	23 36 11.3	26 56 17	-2	15.11	8099	0.2	9.23	9.05	0.56	3.90	20.58	20.29	0.075	104(11)	
330680	23 36 11.6	26 50 30	-2	14.38	9209	0.1	2.75	2.53	0.12	1.09	18.08	17.63	0.065	192	1
330686/476-095A	23 36 13.3	26 56 17	-2	12.41	8891	0.2	14.78	14.66	0.55	6.32	19.87	19.61	0.043	236(19)	
330687	23 36 13.8	26 34 25	-2	13.30	8669	0.2	8.29	8.18	0.34	3.53	19.34	19.08	0.054	212(13)	

TABLE 3. (continued)

Names	RA	Dec	T	m	V_{CMB}	θ	r_e	r_e^c	ϵ_r	R_e	μ_e	μ_e^c	ϵ_μ	σ	ref.
	(1950)	(1950)		mag	km s^{-1}	deg	$''$	$''$	$''$	kpc	– mag/arcsec^2 –			km s^{-1}	
(1)	(2)	(3)	(4)	(5)	(6)	(7)	(8)	(9)	(10)	(11)	(12)	(13)	(14)	(15)	(16)
330691	23 36 18.8	26 50 46	-2	14.59	8645	0.1	5.22	5.07	0.64	2.19	19.03	18.73	0.155	192	1
330696/476-096	23 36 20.3	26 59 26	-5	12.38	8924	0.3	8.83	8.64	0.17	3.73	18.85	18.56	0.026	261(17)	
330699	23 36 23.5	26 46 08	-2	14.87	9298	0.1	1.10	0.74	0.08	0.32	16.39	15.31	0.110	221	1
330700	23 36 25.8	26 53 06	-2	13.93	8872	0.2	3.53	3.34	0.12	1.44	18.28	17.91	0.051	215	1
330706	23 36 32.2	26 49 31	-5	13.77	9594	0.2	4.48	4.31	0.16	1.86	18.74	18.41	0.049	231(17)	*
331248	23 36 41.9	27 16 25	-5	13.39	8922	0.6	8.88	8.63	0.39	3.72	19.66	19.36	0.056	193(13)	
330741/476-101	23 37 18.9	27 05 56	1	12.91	9576	0.5	6.20	5.90	0.20	2.54	18.85	18.49	0.044	187(11)	
330744/476-102	23 37 28.0	26 33 25	-2	12.81	8347	0.4	11.24	10.93	0.52	4.71	19.78	19.49	0.059	202(12)	
U12727/N7728	23 37 30.3	26 51 22	-5	11.18	9052	0.4	21.11	20.95	0.28	9.03	19.60	19.33	0.015	338(16)	
330747	23 37 33.6	26 51 24	-5	15.21	9454	0.4	7.30	6.94	0.85	2.99	18.71	18.50	0.200	107(11)	*
330754/476-105	23 37 48.5	27 17 03	-2	12.13	8323	0.7	18.18	17.99	0.45	7.76	20.27	20.02	0.029	229(14)	
331260	23 38 03.0	26 57 53	-5	13.19	10482	0.5	10.15	9.84	0.44	4.24	19.95	19.62	0.056	197(12)	
U12733/476-107	23 38 15.5	26 33 30	-5	11.99	11359[a]	0.6	22.06	21.89	0.61	9.44	20.47	20.17	0.032	233(14)	
330763/476-109	23 38 23.6	27 13 55	-5	12.88	9626	0.7	8.79	8.45	0.27	3.64	19.51	19.18	0.040	225(13)	
U12744/N7735	23 39 42.0	25 57 00	-5	11.98	9249	1.2	19.68	19.63	0.35	8.47	20.25	20.01	0.020	260(13)	*
U12745/N7737	23 40 12.0	26 46 00	0	12.09	7279[b]	1.0	12.05	11.96	0.22	5.16	19.25	19.03	0.022	251(11)	
330785/476-120	23 40 25.2	27 11 40	0	12.12	7271[b]	1.1	12.43	12.15	0.27	5.24	19.47	19.21	0.028	234(11)	
331298	23 40 44.8	27 05 12	-5	13.05	7431[b]	1.1	7.55	7.17	0.22	3.09	19.05	18.72	0.038	156(11)	
330798/476-123	23 41 00.0	27 02 00	-2	12.41	8781	1.2	22.96	22.92	0.96	9.88	20.12	19.88	0.048	272(14)	
330889/477-004	23 43 18.0	27 04 00	1	13.48	8807	1.7	14.39	14.28	0.65	6.16	20.34	20.08	0.051	114(15)	
331345	23 45 27.8	27 16 30	0	14.14	8108	2.2	122.41	122.41	5.65	52.79	22.63	22.52	0.034	111(11)	
U12785/477-008	23 45 30.0	27 06 00	-2	12.60	8029	2.2	31.01	31.01	0.98	13.37	20.50	20.29	0.032	235(11)	

[a]Probable member of background group (see text)
[b]Probable member of foreground group (see text)

References for Table 3.

1: Lucey et al. 1991a

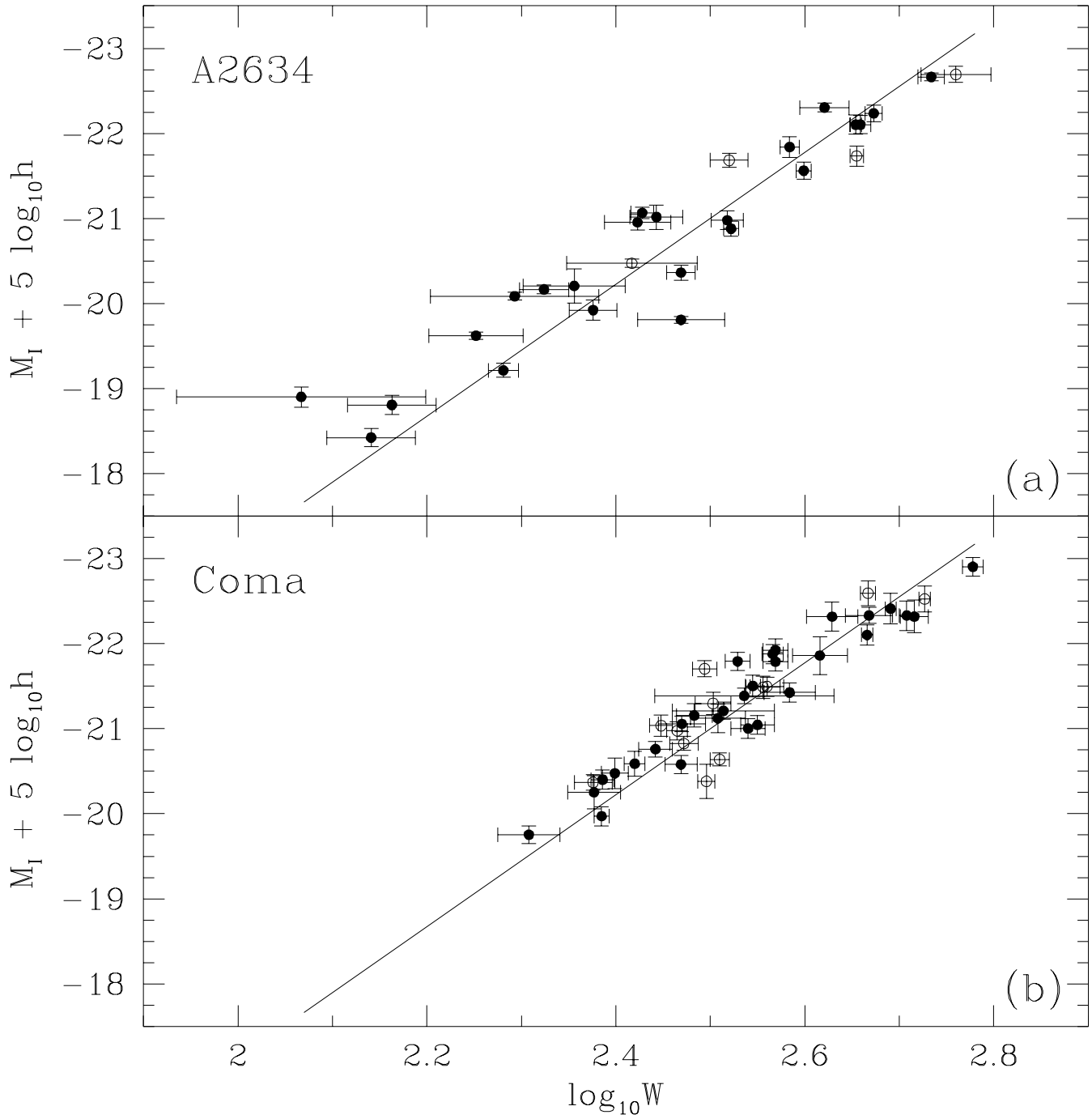
A2634
Coma
(a)
(b)
$M_I + 5\ \log_{10} h$
$\log_{10} W$
−23
−22
−21
−20
−19
−18
2
2.2
2.4
2.6
2.8

TABLE 4. Coma FP data

Names	RA	Dec	T	m	V_{CMB}	θ	r_e	r_e^c	ϵ_r	R_e	μ_e	μ_e^c	ϵ_μ	σ	ref.
	(1950)	(1950)		mag	km s^{-1}	deg	$''$	$''$	$''$	kpc	– mag/arcsec^2 –			km s^{-1}	
(1)	(2)	(3)	(4)	(5)	(6)	(7)	(8)	(9)	(10)	(11)	(12)	(13)	(14)	(15)	(16)
221044/159-083	12 47 14.9	27 09 55	-5	12.30	7155	2.4	9.23	9.03	0.21	3.15	18.86	18.66	0.030	210	2
U7986/N4715	12 47 31.6	28 05 41	1	11.87	7218	2.1	17.12	17.00	0.47	5.92	20.26	20.10	0.034	225	2
221057/159-089	12 48 27.8	28 06 49	-5	12.72	7874	1.9	7.59	7.36	0.20	2.56	19.08	18.86	0.035	176	2
221100/I832	12 51 33.0	26 42 57	-5	12.59	7362	2.0	7.95	7.77	0.17	2.71	19.00	18.81	0.029	217	2
U8028/N4789	12 51 53.3	27 20 20	-5	11.14	8637	1.5	16.43	16.33	0.22	5.69	19.05	18.87	0.016	272	2
U8038/N4798	12 52 29.0	27 41 11	-2	15.10	8119	1.2	46.96	46.96	1.47	16.36	21.19	21.04	0.033	169(14)	
U8049/N4807	12 53 03.6	27 47 30	-5	12.29	7247	1.0	7.05	6.78	0.18	2.36	18.34	18.12	0.035	227(14)	*
221121/I3900	12 53 15.7	27 31 15	-5	12.63	7383	1.1	5.36	5.06	0.23	1.76	17.89	17.60	0.060	280	2
U8057/N4816	12 53 46.7	28 00 56	-5	10.85	7199	0.8	24.60	24.54	0.59	8.55	20.33	20.17	0.028	210	2
221129/160-022	12 53 52.9	26 37 43	-5	12.39	6725	1.8	10.39	10.21	0.31	3.56	19.18	19.01	0.039	269	2
221128/160-023	12 53 54.4	28 01 15	-5	14.02	7171	0.7	12.74	12.62	0.42	4.40	20.51	20.35	0.038	184	2
221134/160-027	12 54 01.3	28 06 01	-5	13.23	6543	0.7	5.51	5.26	0.21	1.83	18.86	18.62	0.053	178	2
221133/N4821	12 54 03.4	27 13 37	-5	13.07	7295	1.2	11.87	11.67	0.35	4.07	19.43	19.25	0.037	169(11)	
U8065/N4827	12 54 18.1	27 26 57	-5	11.81	7878	1.0	12.61	12.43	0.25	4.33	19.18	19.01	0.026	289(19)	2*
221151/160-033	12 54 25.5	27 10 08	-5	13.57	6541	1.2	18.66	18.54	1.05	6.46	20.92	20.77	0.065	85	2
221164/160-037	12 54 44.1	27 44 10	-5	13.02	7748	0.7	4.09	3.87	0.12	1.35	17.89	17.61	0.043	237	2
U8070/N4839	12 54 59.0	27 46 07	-5	9.62	7586	0.7	33.07	33.07	0.35	11.52	20.22	20.07	0.011	245(21)	*
U8072/N4841A	12 55 07.4	28 44 50	-5	12.55	7052	0.7	7.08	6.83	0.18	2.38	18.71	18.57	0.033	264	3*
221175/N4840	12 55 07.6	27 52 57	-5	12.43	6365	0.6	6.81	6.65	0.15	2.32	18.42	18.22	0.029	250	2
U8073/N4841B	12 55 08.9	28 45 08	-5	11.40	7061	0.7	15.92	15.80	0.24	5.50	19.34	19.18	0.018	229	3*
221178/N4842	12 55 10.6	27 45 47	-5	12.75	7585	0.6	5.06	4.86	0.09	1.69	18.10	17.85	0.024	202(14)	
221188/160-049	12 55 23.6	28 27 01	-5	13.61	7513	0.4	3.01	2.61	0.10	0.91	17.61	17.16	0.048	179	2
221193/D238	12 55 29.0	28 46 10	-5	14.06	7607	0.6	3.02	2.67	0.14	0.93	18.07	17.66	0.067	113	2
U8086/N4849	12 55 47.2	26 40 00	-5	11.75	6179	1.6	13.17	13.02	0.22	4.54	19.12	18.98	0.020	215(15)	
221216/160-062	12 55 53.6	29 23 53	-5	13.36	8106	1.2	26.53	26.51	1.34	9.23	21.22	21.05	0.057	128(12)	*
221220/N4850	12 55 56.8	28 14 20	-5	12.90	6312	0.3	6.14	5.94	0.17	2.07	18.65	18.44	0.037	180	2
221226/160-065	12 56 05.3	28 17 09	-5	12.77	7456	0.2	7.39	7.22	0.19	2.52	19.01	18.80	0.034	188	2
221242/N4854	12 56 22.4	27 56 44	-2	12.58	8345	0.3	13.74	13.60	0.41	4.74	20.15	19.96	0.036	175	3
221247/D181	12 56 26.3	28 21 21	-2	14.03	6200	0.2	4.57	4.29	0.42	1.49	18.84	18.53	0.125	142	4
221248/I3947	12 56 27.1	28 03 20	-5	13.49	5945	0.2	5.70	5.49	0.24	1.91	18.71	18.50	0.057	148	2
221252/D136	12 56 30.3	28 14 03	-5	14.35	5936	0.1	1.76	1.30	0.10	0.45	16.89	16.11	0.089	183	5
221256/D135	12 56 35.0	28 14 13	-5	14.42	8588	0.1	4.81	4.59	0.25	1.60	19.56	19.28	0.070	85	2
U8097/N4859	12 56 36.7	27 05 05	-2	12.25	7435	1.2	12.59	12.41	0.36	4.32	19.48	19.32	0.037	217(17)	

TABLE 4. (continued)

Names	RA	Dec	T	m	V_{CMB}	θ	r_e	r_e^c	ϵ_r	R_e	μ_e	μ_e^c	ϵ_μ	σ	ref.
	(1950)	(1950)		mag	km s^{-1}	deg	$''$	$''$	$''$	kpc	– mag/arcsec^2 –			km s^{-1}	
(1)	(2)	(3)	(4)	(5)	(6)	(7)	(8)	(9)	(10)	(11)	(12)	(13)	(14)	(15)	(16)
221259/N4860	12 56 39.0	28 23 38	-5	12.19	8234	0.2	7.85	7.67	0.13	2.67	18.50	18.28	0.022	265	2
221263/I3955	12 56 41.2	28 16 01	-2	12.83	8163	0.1	11.32	11.18	0.43	3.89	19.93	19.74	0.045	181	4
221266/I3957	12 56 42.4	28 02 22	-5	13.57	6644	0.2	4.04	3.70	0.16	1.29	18.47	18.11	0.058	148(12)	*
221267/I3960	12 56 43.0	28 07 33	-2	13.28	6977	0.2	5.07	4.83	0.20	1.68	18.65	18.40	0.054	175	4
221268/I3959	12 56 43.3	28 03 17	-5	12.92	7352	0.2	4.84	4.60	0.11	1.60	18.15	17.88	0.032	195	2
221275/I3963	12 56 48.6	28 02 42	-2	12.96	6943	0.2	13.62	13.48	0.73	4.70	20.43	20.27	0.063	129	4
221274/N4864	12 56 48.9	28 14 41	-5	12.37	7028	0.1	9.12	8.95	0.16	3.12	18.99	18.80	0.022	198	3
221277/N4867	12 56 50.4	28 14 24	-5	13.02	5086	0.1	4.85	4.61	0.13	1.61	18.13	17.90	0.036	222	5
U8100/N4865	12 56 55.1	28 21 16	-5	12.13	4911	0.1	8.89	8.72	0.17	3.04	18.40	18.20	0.025	234	4*
221285/N4869	12 56 56.8	28 10 53	-5	12.39	6971	0.1	8.46	8.29	0.14	2.89	18.84	18.65	0.020	205	3
221284/D106	12 56 58.1	28 10 05	-2	14.07	5360	0.1	3.76	3.47	0.18	1.21	18.67	18.33	0.070	159	4
221289/D67	12 57 00.2	28 00 46	-2	13.86	6276	0.2	3.75	3.39	0.18	1.18	18.21	17.85	0.069	148	4
221291/D157	12 57 00.6	28 14 32	-2	13.76	6351	0.0	6.49	6.27	0.27	2.18	19.54	19.34	0.100	126	4*
221290/D132	12 57 00.8	28 14 23	-2	14.06	7931	0.0	6.91	6.71	0.35	2.34	19.96	19.73	0.100	127	4*
221293/D156	12 57 01.7	28 16 04	-5	14.34	6992	0.0	5.53	5.30	0.25	1.85	19.75	19.52	0.100	109	2*
221295/D177	12 57 04.1	28 18 43	-2	14.57	7139	0.1	7.10	6.90	0.38	2.40	19.84	19.63	0.069	99	4
221296/I3967	12 57 04.6	28 07 11	-5	13.07	7218	0.1	6.44	6.22	0.33	2.17	18.63	18.42	0.070	251	4
221298/N4871	12 57 05.4	28 13 36	-2	13.17	7381	0.0	14.09	13.98	0.42	4.87	20.05	19.88	0.100	168	4*
221301/I3973	12 57 06.2	28 09 08	-2	14.55	5013	0.1	4.05	3.78	0.15	1.32	17.85	17.54	0.051	208	4
221302/D176	12 57 06.9	28 19 05	-2	13.78	5847	0.1	7.80	7.62	0.44	2.65	19.25	19.08	0.071	161	4
221303/N4873	12 57 08.0	28 15 12	-2	13.23	5930	0.0	13.78	13.67	0.38	4.76	20.11	19.96	0.100	150	4*
221304/N4872	12 57 09.7	28 12 55	-5	13.30	7413	0.0	3.55	3.25	0.12	1.13	17.76	17.38	0.100	212	5*
U8103/N4874	12 57 11.1	28 13 48	-5	9.17	7457	0.0	52.91	52.91	0.71	18.43	20.86	20.71	0.013	204(23)	3*
221313/N4875	12 57 13.1	28 10 37	-2	13.40	8165	0.1	4.48	4.23	0.15	1.47	18.36	18.04	0.045	182	4
221317/D128	12 57 15.1	28 13 32	-2	14.77	7949	0.1	7.62	7.43	0.70	2.59	19.95	19.73	0.150	104	4*
221323/160-233	12 57 17.5	28 11 39	-5	14.35	7216	0.1	1.35	0.89	0.08	0.31	16.50	15.48	0.150	183	2*
221329/D153	12 57 18.9	28 15 51	-5	14.03	6908	0.1	2.98	2.62	0.15	0.91	18.18	17.77	0.100	135	5*
221331/N4876	12 57 19.6	28 10 54	-5	13.34	7009	0.1	8.40	8.22	0.22	2.86	19.12	18.93	0.100	195	2*
221332/160-235	12 57 21.3	28 07 36	-2	13.47	8296	0.1	7.79	7.61	0.37	2.65	19.54	19.32	0.061	126	4
221334/D152	12 57 22.5	28 14 46	-2	13.67	9639	0.1	11.42	11.28	0.39	3.93	20.09	19.88	0.100	156	4*
221343/D193	12 57 30.4	28 23 51	-5	14.18	7812	0.2	5.87	5.64	0.29	1.96	19.50	19.26	0.066	120	5
221345/N4883	12 57 31.3	28 18 14	-2	13.16	8229	0.1	8.99	8.82	0.25	3.07	19.34	19.13	0.035	171	4
U8106/N4881	12 57 33.1	28 30 59	-5	12.29	6998	0.3	9.21	9.04	0.20	3.15	19.12	18.93	0.028	210	2

TABLE 4. (continued)

Names	RA	Dec	T	m	V_{CMB}	θ	r_e	r_e^c	ϵ_r	R_e	μ_e	μ_e^c	ϵ_μ	σ	ref.
	(1950)	(1950)		mag	$km\,s^{-1}$	deg	$''$	$''$	$''$	kpc	– mag/arcsec^2 –			$km\,s^{-1}$	
(1)	(2)	(3)	(4)	(5)	(6)	(7)	(8)	(9)	(10)	(11)	(12)	(13)	(14)	(15)	(16)
221354/N4886	12 57 39.8	28 15 27	-5	12.78	6665	0.1	9.37	9.20	0.28	3.20	19.59	19.41	0.100	148(13)	*
221357/D65	12 57 41.6	28 02 46	-2	13.05	6321	0.3	15.35	15.25	0.48	5.31	20.68	20.53	0.036	115	4
221362/I4011	12 57 41.8	28 16 23	-5	14.03	7410	0.1	5.85	5.62	0.34	1.96	19.35	19.12	0.100	106	5*
U8110/N4889	12 57 43.0	28 14 46	-5	9.68	6785	0.1	35.74	35.74	0.33	12.45	19.61	19.47	0.010	445(40)	*
221364/I4012	12 57 43.3	28 20 51	-5	13.63	7486	0.2	2.97	2.61	0.11	0.91	17.44	17.02	0.054	179	5
221365/D207	12 57 44.4	28 26 22	-5	13.39	7032	0.2	7.46	7.27	0.24	2.53	19.39	19.18	0.041	147	5
221372/D173	12 57 48.4	28 20 48	-2	13.84	7652	0.2	4.51	4.26	0.23	1.48	18.70	18.39	0.072	137	4
221376/I4021	12 57 50.1	28 18 36	-5	13.61	6057	0.2	3.69	3.40	0.16	1.18	18.24	17.89	0.062	158	5
221377/N4894	12 57 51.8	28 14 10	-2	14.01	4855	0.2	14.25	14.14	0.85	4.93	20.50	20.38	0.100	91	4*
221380/N4898A	12 57 52.9	28 13 28	-5	12.35	7116	0.2	8.53	8.36	0.21	2.91	18.64	18.45	0.100	201	5*
221382/N4898B	12 57 53.3	28 13 31	-5	14.19	6617	0.2	2.09	1.61	0.11	0.56	17.33	16.64	0.100	140	5*
U8113/N4895	12 57 53.5	28 28 09	-2	11.34	8674	0.3	24.41	24.37	0.59	8.49	19.77	19.58	0.026	213	4
221386/I4026	12 57 57.6	28 18 57	-2	13.24	8457	0.2	8.24	8.06	0.28	2.81	19.61	19.39	0.043	140	4
221390/D27	12 58 02.0	27 47 04	-5	13.81	8093	0.5	6.15	5.93	0.27	2.07	19.56	19.33	0.058	106	2
221392/D119	12 58 03.5	28 13 38	-2	13.83	7195	0.2	5.55	5.32	0.27	1.85	19.44	19.11	0.064	153	4*
221403/160-251	12 58 11.2	28 24 49	-2	13.93	5794	0.3	53.42	53.42	5.17	18.61	21.80	21.68	0.087	91	4
221404/D146	12 58 14.6	28 17 08	0	12.78	7288	0.3	20.17	20.08	0.73	6.99	21.10	20.94	0.038	105	4
221408/N4906	12 58 14.9	28 11 31	-5	12.87	7773	0.3	7.36	7.17	0.19	2.50	19.03	18.81	0.034	168	3
221410/I4041	12 58 16.5	28 15 57	-5	16.98	7358	0.3	12.70	12.58	0.36	4.38	20.14	19.97	0.034	116(11)	*
221412/I4042	12 58 18.2	28 14 22	-2	12.84	6523	0.3	6.29	6.07	0.24	2.11	18.66	18.45	0.051	162	4
221413/D116	12 58 18.5	28 14 04	-2	13.50	8634	0.3	7.08	6.88	0.29	2.40	19.53	19.30	0.054	130	4
221416/D191	12 58 20.4	28 22 08	-2	14.52	6879	0.3	15.67	15.57	1.81	5.42	20.70	20.54	0.127	89	4
221419/I4045	12 58 24.2	28 21 31	-5	12.55	7123	0.3	7.52	7.33	0.18	2.55	18.52	18.31	0.031	211	5
221420/N4908	12 58 26.9	28 18 35	-5	12.39	9010	0.3	8.48	8.31	0.20	2.89	18.74	18.51	0.031	206	2
221422/160-091	12 58 27.7	28 38 03	-2	12.35	7915	0.5	10.93	10.76	0.27	3.75	19.32	19.13	0.031	202(13)	
U8129/I4051	12 58 29.8	28 16 40	-5	11.84	5232	0.3	21.01	20.93	0.40	7.29	20.25	20.13	0.021	223	3
221429/160-261	12 58 34.7	28 10 04	0	13.61	7175	0.3	21.38	21.31	1.05	7.42	20.61	20.45	0.052	147	4
221434/160-092	12 58 44.8	28 05 13	-5	13.75	6243	0.4	6.73	6.52	0.32	2.27	19.69	19.50	0.063	158	2
U8133/N4919	12 58 53.4	28 04 28	-2	12.48	7568	0.4	9.51	9.33	0.23	3.25	18.97	18.77	0.032	164(12)	*
221438/D204	12 58 58.3	28 27 53	-5	13.75	7935	0.5	5.24	5.00	0.21	1.74	19.07	18.84	0.055	135	2
221442/N4923	12 59 07.4	28 06 52	-5	12.33	5793	0.5	6.43	6.19	0.12	2.16	18.38	18.18	0.025	209	2
U8137/I843	12 59 09.5	29 23 58	-5	11.88	7655	1.2	15.88	15.76	0.49	5.49	19.34	19.18	0.041	248	2
221453/160-100	12 59 25.9	28 09 43	-5	13.54	7872	0.5	3.64	3.34	0.15	1.16	18.25	17.86	0.060	192	2

TABLE 4. (continued)

Names	RA	Dec	T	m	V_{CMB}	θ	r_e	r_e^c	ϵ_r	R_e	μ_e	μ_e^c	ϵ_μ	σ	ref.
	(1950)	(1950)		mag	km s^{-1}	deg	$''$	$''$	$''$	kpc	– mag/arcsec^2 –			km s^{-1}	
(1)	(2)	(3)	(4)	(5)	(6)	(7)	(8)	(9)	(10)	(11)	(12)	(13)	(14)	(15)	(16)
U8142/N4926	12 59 29.2	27 53 26	-5	11.74	8142	0.6	9.15	8.97	0.15	3.12	18.47	18.26	0.022	266	2
221455/N4927	12 59 33.2	28 16 27	-5	12.12	8015	0.6	11.58	11.44	0.28	3.98	19.17	18.98	0.031	292	2
230015/N4929	13 00 20.1	28 18 48	-5	12.69	6502	0.7	9.23	9.07	0.21	3.16	19.45	19.27	0.029	191	2
U8154/N4931	13 00 36.5	28 18 02	-2	11.86	5686	0.8	11.42	11.30	0.45	3.94	18.46	18.30	0.050	205(12)	
U8167/N4944	13 01 25.9	28 27 13	-2	11.86	7256	1.0	33.48	33.48	0.59	11.66	19.91	19.76	0.019	198(13)	
230042/I4133	13 01 26.6	28 15 21	-5	13.22	6645	1.0	3.93	3.62	0.16	1.26	18.14	17.78	0.057	178	2
U8175/N4952	13 02 34.8	29 23 25	-5	11.53	6231	1.7	12.90	12.77	0.20	4.45	18.81	18.66	0.019	228(15)	2*
U8178/N4957	13 02 48.2	27 50 14	-5	11.64	7190	1.3	17.66	17.55	0.29	6.11	19.70	19.54	0.020	249	2
230086/N4971	13 04 31.7	28 48 53	-5	12.60	6560	1.7	7.81	7.58	0.26	2.64	18.91	18.71	0.044	184	2
U8260/N5004	13 08 39.2	29 54 08	-5	11.65	7329	3.0	11.76	11.58	0.19	4.03	18.80	18.63	0.020	244	2

References for Table 4.

2 : Lucey et al. 1991b
3 : Faber et al. 1989
4 : Dressler 1987
5 : Davies et al. 1987

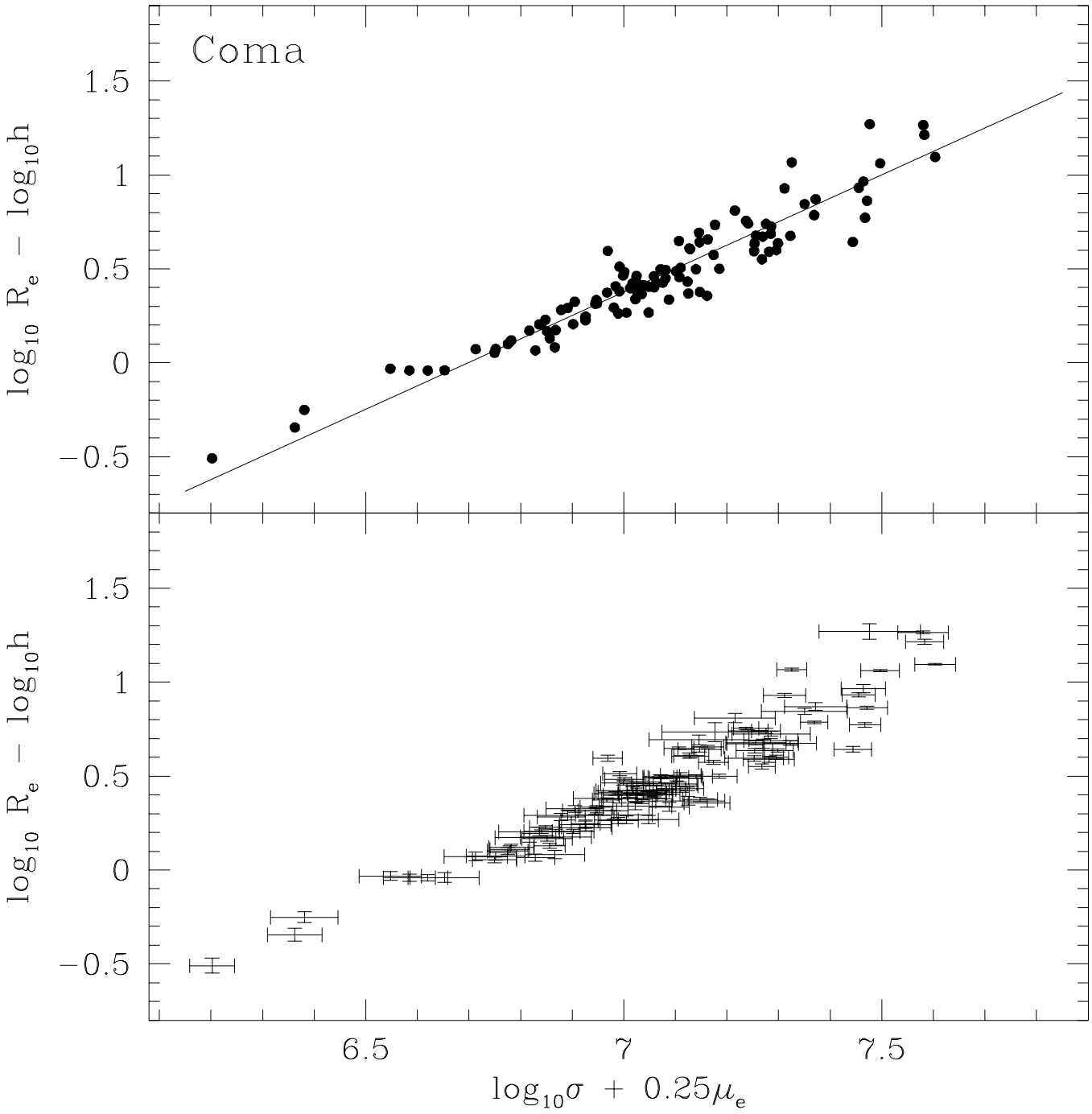
Coma
1.5
1
0.5
0
−0.5
log10 Re − log10h
6.5
7
7.5
log10σ + 0.25μe

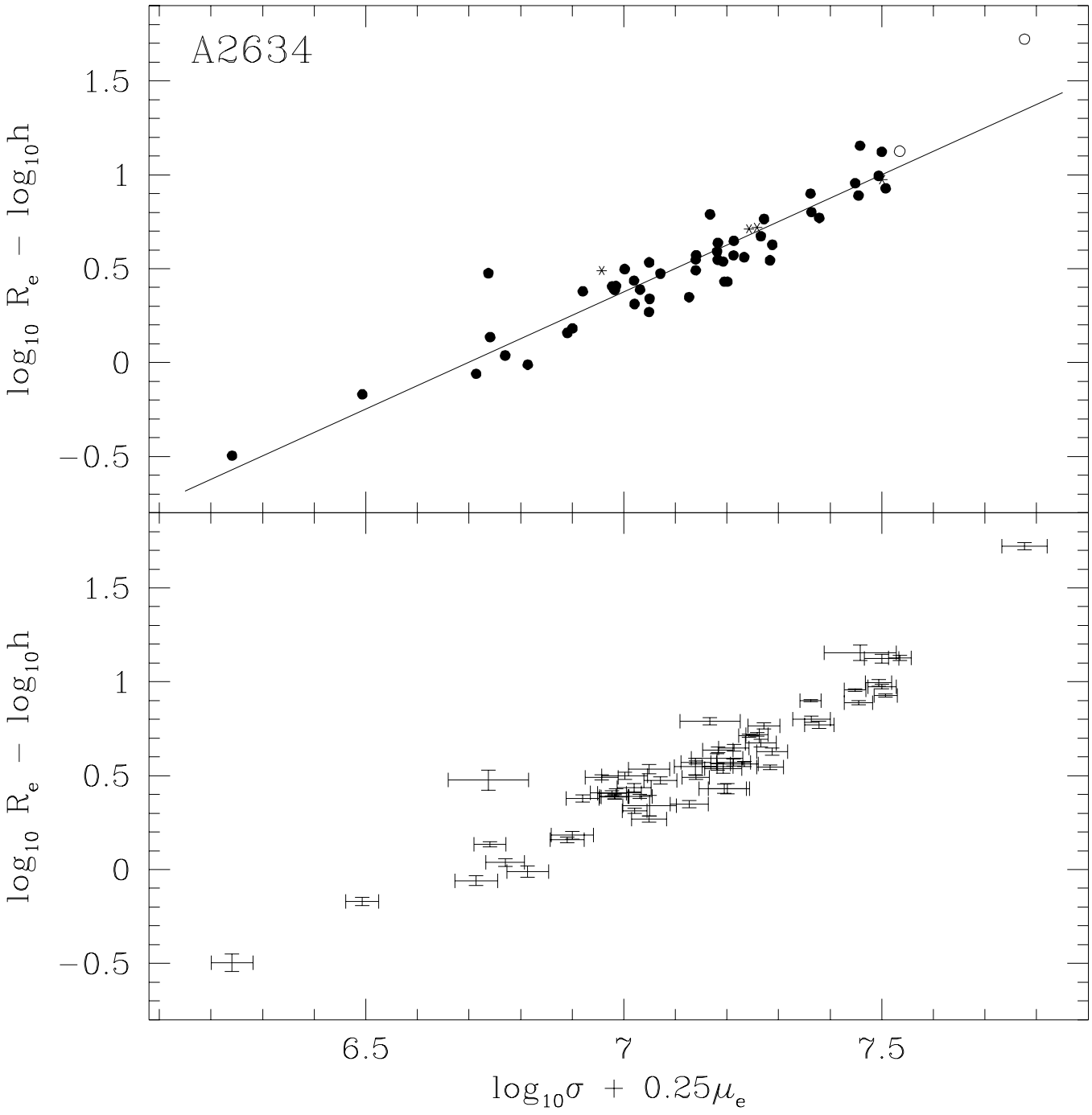
A2634
1.5
1
0.5
0
−0.5
log10 Re − log10h
6.5
7
7.5
log10σ + 0.25μe